AD-A149 380

PROGRESS REPORT

RESEARCH ON RAPIDLY SOLIDIFIED ALLOYS

D. SHECHTMAN AND L. A. BENDERSKY

THE JOHNS HOPKINS UNIVERSITY
CENTER FOR MATERIALS RESEARCH
G. W. C. WHITING SCHOOL OF ENGINEERING
BALTIMORE, MARYLAND 21218

DTIC FILE COPY

APPROVED FOR PUBLIC RELEASE
DISTRIBUTION UNLIMITED

DTIC
ELECTE
JAN 2 1985
S D
D

DARPA ORDER NO. MDA 903-83-K-0400
EFFECTIVE DATE: 08-05-83
EXPIRATION DATE: 08-04-85
SPONSORED BY: DEFENSE ADVANCED RESEARCH PROJECTS AGENCY (DARPA)

NOVEMBER 1984

84 12 20 015

SECURITY CLASSIFICATION OF THIS PAGE (When Data Entered)

REPORT DOCUMENTATION PAGE		READ INSTRUCTIONS BEFORE COMPLETING FORM
1. REPORT NUMBER CMR-DARPA-9	2. GOVT ACCESSION NO. AD-A149380	3. RECIPIENT'S CATALOG NUMBER
4. TITLE (and Subtitle)		5. TYPE OF REPORT & PERIOD COVERED Progress Report 11-1-83 to 11-1-84
		6. PERFORMING ORG. REPORT NUMBER
7. AUTHOR(s) D. Shechtman and L. A. Bendersky		8. CONTRACT OR GRANT NUMBER(s) MDA-903-83-K-0400
9. PERFORMING ORGANIZATION NAME AND ADDRESS The Johns Hopkins University Center for Materials Research Baltimore, Maryland 21213		10. PROGRAM ELEMENT, PROJECT, TASK AREA & WORK UNIT NUMBERS
11. CONTROLLING OFFICE NAME AND ADDRESS DARPA 1400 Wilson Blvd. Arlington, Va. 22209		12. REPORT DATE November 1984 13. NUMBER OF PAGES 90
14. MONITORING AGENCY NAME & ADDRESS(if different from Controlling Office) ONRRR George Washington University 2110 G Street, SW Washington, D. C. 20037		15. SECURITY CLASS. (of this report) A 15a. DECLASSIFICATION/DOWNGRADING SCHEDULE

16. DISTRIBUTION STATEMENT (of this Report)

Approved for public release, distribution unlimited

17. DISTRIBUTION STATEMENT (of the abstract entered in Block 20, if different from Report)

18. SUPPLEMENTARY NOTES

19. KEY WORDS (Continue on reverse side if necessary and identify by block number)

preparation, characterization of rapidly solidified alloys; NiAl-Cr, Al-Mn, Al-Cu, $Al_9(Fe,Ni)_2$.

20. ABSTRACT (Continue on reverse side if necessary and identify by block number)

The report describes the study of rapidly solidified alloys including methods of preparation, processing and characterization using a variety of techniques such as TEM, analytical electron microscopy, and x-ray diffraction.

DD FORM 1 JAN 73 1473 EDITION OF 1 NOV 65 IS OBSOLETE

TABLE OF CONTENTS:

Accession For	
NTIS GRA&I	☒
DTIC TAB	☐
Unannounced	☐
Justification	
By	
Distribution/	
Availability Codes	
Dist	Avail and/or Special
A/1	

DTIC COPY INSPECTED 4

EXECUTIVE SUMMARY

This progress report covers the research results accomplished by The Johns Hopkins University Center for Materials Research under DARPA contract No. MDA903-83-K-0400 on "Characterization of Rapidly Solidified Alloys" and reported at national scientific and engineering meetings during the period November 1983 to November 1984. The research program has already produced ten progress reports to the sponsor and seventeen manuscripts which have been published or are in preparation to be submitted for publication.* Communication of scientific and engineering results is an important part of the research process and therefore the assembling of the papers included in this report under one cover was judged to be useful to the materials community. The fine contributions of the principal investigator, Dr. Dan Shechtman, and the co-investigator, Dr. Leonid Bendersky, merit special acknowledgement.

Emanuel Horowitz, Director
Center for Materials Research
The Johns Hopkins University

*See Appendix I.

RAPID SOLIDIFICATION MICROSTRUCTURES AND PRECIPITATES IN Aℓ-Mn ALLOYS

R. J. SCHAEFFER,* D. SHECHTMAN,** AND F. S. BIANCANIELLO*

*National Bureau of Standards, Washington, D. C. 20234

**Technion, Haifa, Israel and Center for Materials Research, Johns Hopkins University, Baltimore, Md. 21218

Published in the Proceedings of the Materials Research Society Meeting, Boston, Ma., November 1983.

ABSTRACT

Rapidly solidified Al containing up to to 15 wt.% Mn was prepared by melt spinning. The alloys were examined by TEM and X-ray diffraction in the as-spun condition and after annealing at 450°C. Four precipitate phases were detected, and their growth kinetics were correlated to subgrain structures in the Al matrix.

INTRODUCTION

It has long been known that solid solutions containing far more than the limiting equilibrium concentration (1.4 wt.%) of Mn in Al can be obtained by rapid solidification [1]. Such solubility extensions in Al have been observed for almost every solute which has been investigated [2].

On the basis of interface equilibrium, the theory of morphological stability predicts an absolute stability regime in which plane-front microsgregation-free solidification of an alloy is stabilized by surface energy effects at sufficiently high solidification velocities. In the aluminum-manganese system the velocity required to produce this effect is predicted to be relatively low (a few centimeters per second) because of the high value of the solute partition coefficient [3]. In contrast, solutes with low distribution coefficients (Fe, Ni, Co, etc.) are predicted to be destabilizing at concentrations $<<1$ wt.% at comparable solidification velocities. Quantitative verification of the absolute stability effect has been observed in Ag-Cu alloys [4] but has not been reported for Al-based alloys. At solidification velocities approaching 1 m/s or greater, it is expected that interface equilibrium is no longer maintained, and microsegregation-free solidification can be attained even in systems having very low equilibrium partition coefficients [5].

When plane-front solidificaiton is not stable, a cellular or dendritic interface develops and the solid which is generated contains a pattern of microsegregation. A network of crystal sub-boundaries can develop coincident with the microsegregation pattern, because of crystallographic mismatch between adjacent cells or dendrites.

During the annealing of supersaturated Al-Mn alloys the G phase, with composition corresponding to $Al_{12}Mn$ and usually considered to be metastable, appears and at temperatures below about 500° C can persist for long times in samples which also contain the Al_6Mn phase [6]. In addition, Nes et al. [7] have reported two other metastable phases in Al-1.8 wt.% Mn annealed at 460° C. One phase, designated G', had a simple cubic structure, and the other phase, designated G", had an hexagonal lattice with $c/a = 1.04$.

Unfortunately, none of the previous studies of precipitation in this system has covered the wide range of solid solution compositions which is attainable by rapid solidification. In this paper we report a study of precipitation at 450° C in melt-spun ribbons of Al-Mn containing up to 15 wt.% Mn.

EXPERIMENT

Melt-spun ribbons, typically 2 mm wide and 40-50 μm thick, were prepared from 99.999% Al and 99.95% Mn. Samples were annealed at 450° C for periods ranging from 5 minutes to 92 hours. Details of preparation are reported elsewhere [8]. Lattice parameters and the relative abundance of precipitate phases were determined from X-ray diffractometer measurements. Microstructural studies were performed in a 120 kv scanning transmission electron microscope.

RESULTS

Crystal Phases

In addition to the Al matrix, four phases have been identified by TEM in the as-spun or the annealed ribbons. The Al_6Mn phase is seen as generally globular particles with no preference in growth direction within the aluminum matrix. This phase occurs either on subgrain boundaries or within the subgrains depending upon composition and heat treatment. The G phase is semicoherent with the aluminum matrix and therefore is surrounded by misfit dislocations. The hexagonal G" phase is faulted parallel to the basal plane, and the plate normal of the particles is parallel to the c direction. The T phase, which does not correspond to any previously reported phase, has the shape of an elongated plate and contains a complex faulted structure on planes perpendicular to its length. The G' phase of Nes et al. [7], which was believed to be associated with impurities, was not detected in our samples.

The X-ray diffraction charts show only peaks corresponding to reflections reported in the literature for Al_6Mn [9] and the G phase [6, 10, 11, 12], as well as Al.

As-spun Ribbons

At low Mn concentrations, the ribbons consist of cell-free grains containing a high dislocation density but no evidence of microsegregation. In the higher composition alloys, a cellular microstructure is present, with unidentified fine precipitates at the cell boundaries and a contrast difference between the cells indicating that the cell boundary is also a subgrain boundary. The transition from cell-free to cellular structures occurs at about 5 wt.% Mn. At this composition, two different ribbons were produced by varying the parameters of the melt spinning process. A thinner ribbon (35 μm maximum thickness) was free of cells while a thicker (55 μm) ribbon, which may have solidified more slowly, contained a cellular substructure.

The measured lattice parameters (Fig. 1) of the as-spun ribbons decrease with increasing Mn concentration as reported in several previous studies [1,13, 14,15], but in the cellular samples the decrease is not as large as would be expected if all of the Mn were in solid solution. In the 15 wt.% Mn ribbon diffraction peaks corresponding to two different concentrations of Mn in solution in Al are seen. These concentrations, approximately 14 and 3 wt.% Mn, correspond to a supersaturated cellular region and a two-phase solidification region respectively.

Annealed Ribbons

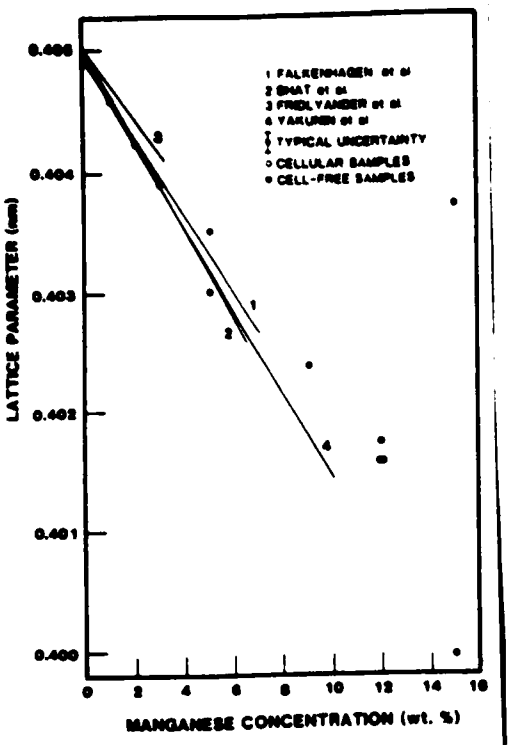

FIG. 1. Lattice parameters of as-spun Al-Mn ribbons compared to results of Falkenhagen et al.[1], Bhat, et al.[15], Fridlyander et al.[13], and Yakunin et al.[14].

At 450° C, the supersaturation of the alloys containing 5 wt.% Mn or more disappears rapidly. In contrast, the supersaturation of the alloys with 3 wt.% Mn or less diminishes over a period of many hours (Fig. 2). X-ray diffraction peaks from Al_6Mn are seen within one hour but the G phase peaks appear only after several hours. The G phase peaks increase in intensity with annealing time, while the Al_6Mn peaks diminish with time for anneals longer than 16 hours. On this basis, it appears that G is slightly more stable than Al_6Mn at 450° C. This is not inconsistent with the observations of other workers [6,16] who have investigated precipitation at this temperature in the Al-Mn system and have concluded that Al_6Mn is stable at high temperatures while the G phase persists for long times [6] or becomes stable [16] as the temperature decreases.

By TEM it is found that the location and growth kinetics of the different precipitating phases which form when the ribbons are annealed at 450° C are strongly correlated to the networks of subgrain boundaries which are present in the ribbons. These subgrain boundaries are already seen in the as-spun ribbons at higher concentrations and are considered to be the result of the cellular solidification process. In the less concentrated alloys, where no cellular solidification structure is present, subgrain boundaries may be generated by polygonization.

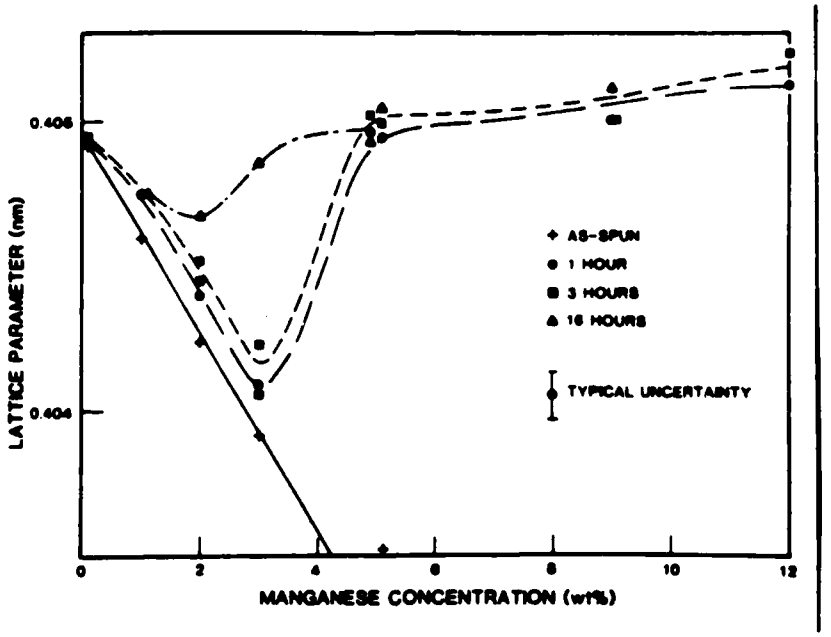

FIG. 2. Lattice parameter of Al-Mn ribbons at different annealing times.

In the 3 wt.% Mn alloy elongated particles of Al_6Mn are seen along subgrain boundaries after 1 hour at 450° C. The subgrains contain a high density of dislocations but only widely scattered precipitates. After 92 hours at 450° C, three precipitate phases are seen. All of them, including Al_6Mn, are now seen within the subgrains, possibly as a result of boundary migration. G phase particles, globular in shape, are surrounded by misfit dislocations indicating a high degree of coherence with the Al matrix. The G" Phase was in the form of elongated particles up to 2 μm in length.

The 5 wt.% Mn ribbons also showed Al_6Mn particles along the subgrain boundaries after being annealed for 1 hour. In addition, the interior of the subgrains showed a diffused population of T phase platelets except in a depleted zone adjacent to the subgrain boundaries (Fig. 3). In the thick ribbon, the Al_6Mn particles were more globular and the zone depleted of T particles was wider than in the thin ribbon. At longer annealing times considerable coarsening of the precipitate particles is seen.

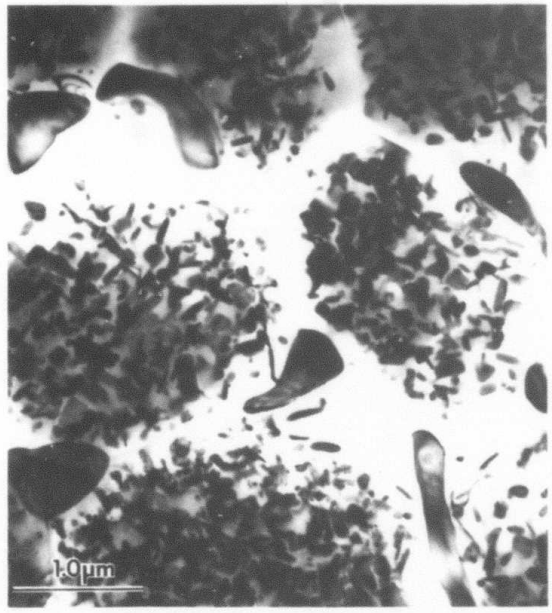

FIG. 3. Al-5 wt.% Mn alloy following 1 hour anneal at 450°C.

The 9 wt.% Mn ribbon was examined after a 5 minute anneal and it was found that a globular phase was present along the subgrain boundaries and a needle-like phase was present within the subgrains. These phases could not be identified. The needle-like phase diminished in abundance as the annealing time increased, and after 16 hours it was found that Al_6Mn particles about 0.5 μm long were dispersed within the subgrains while large G phase particles outlined many of the subgrain boundaries.

At 12 wt.% Mn, a 1 hour anneal resulted in the formation of globular Al_6Mn particles within the Al matrix. After 22 hours at 450° C the microstructure consisted of an aluminum phase containing Al_6Mn particles and a G phase containing a low density of aluminum inclusions.

DISCUSSION

The microsegregation-free ribbons produced at compositions up to 5 wt.% Mn can be taken as evidence for a plane-front solidification process which is predicted by the theory of morphological stability to be stabilized at high solidification velocities. No quantitative correlation is possible because the actual velocities of solidification are not known. The onset of a cellular solidification process with increasing Mn content does not

preclude further increases in the supersaturation of the Al phase, but it does result in a microstructure containing a cellular array of subgrain boundaries which play an important role in subsequent precipitation processes.

Upon annealing at 450° C, precipitates lying along subgrain boundaries grow most rapidly. In the alloys containing 5 wt.% Mn or more, a high density of precipitates is seen within the subgrains but a denuded zone is present near the subgrain boundaries. These observations suggest that the subgrain boundaries serve as paths of rapid diffusion during the precipitation process.

In alloys containing 3 wt.% Mn or less, very few precipitates are formed within the grain and the supersaturation can thus persist for long times.

The G" phase and the T phase apparently occur only with a limited range of composition, and do not attain a sufficiently high volume fraction to be observed by X-ray diffraction. The G phase appears to be more stable than Al_6Mn at 450°C.

ACKNOWLEDGEMENT

This work was supported by DARPA.

REFERENCES

1. G. Falkenhagen and W. Hofman, Z. Metal. 43, 69 (1952).
2. H. Jones, Aluminium 54, 274 (1978).
3. R.J. Schaefer, S.R. Coriell, R. Mehrabian, C. Fenimore and F.S. Biancaniello, in Rapidly Solidified Amorphous and Crystalline Alloys, B.H. Lear, B.C. Giessen, and M. Cohen, eds., North Holland, New York, p. 79, 1982.
4. W.J. Boettinger, D. Shechtman, R.J. Schaefer, and F.S. Biancaniello, Met. Trans (in press).
5. J. Narayan, J. Appl. Phys. 52, 1289 (1981).
6. K. Little, G.V. Raynor, and W. Hume-Rothery, J. Inst. Met. 73, 83 (1946).
7. E. Nes, S.E. Naess, and R. Hoier, Z. Metal. 63, 248 (1972).
8. D. Shechtman, R.J. Schaefer, and F.S. Biancaniello, to be published.
9. A.D.I. Nicol, Acta Cryst. 6, 285 (1953).
10. K. Little and W. Hume-Rothery, J. Inst. Met. 74, 521 (1948).
11. G. Marchand, J. Inst. Met. 73, 747 (1947).
12. J. Adam and J.B. Rich, Acta Cryst. 7, 813 (1954).
13. I.N. Fridlyander, V.A. Konstantinov, and N.I. Zaitseva, Zhurnal Fizicheskoi Khimii, 30 (7), 1623 (1956).
14. A.A. Yakunin, I.I. Osipov, V.I. Tkach, and A.B. Lysenko, Fiz. Metal. Metalloved 43, 140 (1977).
15. S.P. Bhat, T.R. Ramachandran, and A.K. Jena, J. Mat. Sci. 9, 1759 (1974).
16. K. Kusumoto and M. Ohta, Journ. Inst. Polytechn. Osaka Univ. 5 (6), 57 (1954); Nippon Kinzoku Gakki-Si 18 (8), 466 (1954).

MICROSTRUCTURE OF SUPERCOOLED SUB-MICROMETER ALUMINUM-COPPER ALLOY POWDER

S. D. RIDDER* AND D. SHECHTMAN**

*Metallurgy Division, National Bureau of Standards, Washington, D. C. 20234

**Center for Materials Research, Johns Hopkins University, Baltimore, Md. 21218

Published in the Proceedings of the American Society for Testing and Materials (ASTM) Conference on "Rapidly Solidification of Aluminum Powders," Philadelphia, Pa., April 1984.

ABSTRACT

Various Al-Cu alloy powder particles were produced by Electrohydrodynamic (EHD) atomization. The particles produced by this process range in size from 3 nm to 2 μm. The microstructure of the sub-micrometer particles is shown as well as a discussion of their cooling rates and solidification history.

The alloys produced included various compositions of Al-Cu. Extended solid solubility was observed in all alloys, dependent on particle size (the extent of bulk undercooling before solidification ensues is presumed to increase with decreasing particle size) and concentration. The particles produced from alloy concentrations beyond the equilibrium solubility limit which exhibit segregation-free microstructure most likely solidified after undercooling sufficiently to produce the interfacial temperatures and velocities necessary to suppress segregated growth. These aspects of solidification will be discussed and estimates of cooling rates and bulk undercoolings achieved will be given. Some of the particles show a transition from partitionless solidification to a segregated, cellular solidification mode.

Key Words: sub-micrometer particles, aluminum-copper alloys, microstructure, solidification, supercooling.

Introduction

Electrohydrodynamic (EHD) atomization has provided the materials scientist with a means of producing submicron sized particles of various compositions. These micro "castings" are generally transparent to the 100 keV electrons used in conventional TEM analysis allowing one to see the entire solidification structure. This paper will discuss the various microstructures observed in a series of aluminum-copper alloys produced by EHD atomization. In particular, the formation of metastable solutions in many of these particles will be related to the initial composition and apparent degree of bulk supercooling achieved prior to the onset of solidification. Some particles exhibited a transition from partitionless (massive) solidification to a segregated, cellular type solidification mode as described earlier by Levi and Mehrabian [1], Cohen and Mehrabian [2], and Shechtman, Ridder, and Mehrabian [3].

Experimental Procedure

The Al-Cu binary alloy particles were produced by EHD atomization at the National Bureau of Standards (NBS). The material to be atomized was prealloyed by vacuum arc melting appropriate quantities of high purity melt stock (99.999% Al and 99.999% Cu) and cutting into pieces approximately 13 mm in diameter and 15 mm long. These were placed in the EHD atomizing chamber and atomized at an extraction voltage of 12-14 kV and a feed pressure of 3 to 15 kPa (20 to 115 Torr) versus the 1×10^{-4} Pa (10^{-6} Torr) pressure in the atomizing chamber. A schematic of the EHD atomizing system is shown in Figure 1. The atomized particles solidified in flight and were collected

on acetate tape. The acetate was coated with carbon and processed by standard replication foil techniques so as to produce TEM grids with the particles imbedded in the carbon film.

Results and Discussion

The particles produced were divided into two types; ones which exhibited segregation-free microstructure, as shown in Figure 2(a) and ones which exhibited a segregated, cellular microstructure, as shown in Figure 2(b). These types of microstructures have previously been reported in fine powders of Al-Si and Al-Cu alloys [1, 2].

Most of the Al-Cu particles studied were in the size range of 3 nm to 2 μm. In general, larger particles did not solidify in flight. Furthermore, particles larger than ~ 2 μm are not transparent to 100 keV electrons.

The degree of undercooling and the composition determine whether the whole particle is subjected to partitionless solidification or only a part of it, in which case cellular microstructure will form in the last solidification stage. The microstructure developed as a function of size and composition was studied on a large number of particles of each composition and the results are given in Figure 3. Particles having compositions of 2 wt% Cu and less, and with sizes less than 1.4 μm do not contain cells (larger particles could not be studied because of lack of transparency). Cellular structure was detected in particles larger than 1.1 μm at 3 wt% Cu, but at 4.5 wt% Cu this size drops to 0.5 μm, and continues to drop to 0.2 μm at 20 wt% Cu. The size at which the transition from partitionless to cellular occurs at each composition can be determined rather precisely, and as can be seen in Figure 3 no size overlap is observed in which partitionless particles and cellular ones occur simultaneously. This indicates a very

strong dependence of the degree of undercooling on the size, as predicted by theory.

These observations can be interpreted in terms of bulk supercooling prior to nucleation and interfacial temperatures and velocities during solidification. Although partitionless solidification is possible without undercooling the liquid [4], it is reasonable to assume that substantial undercoolings will be achieved in these μm sized particles where cooling rates due to radiation are on the order of 10^5°C per second. Considering the case of growth into undercooled melts, partitionless solidification requires an interfacial temperature below the $T_o^{L/\alpha}$ temperature of the alloy (the $T_o^{L/\alpha}$ temperature is that point at which the α-solid and liquid have the same free energy) and an interfacial velocity in excess of the diffusive velocity of solute in the liquid in front of the interface. For powder particles, the latter conditions can only be achieved through substantial bulk supercoolings prior to solidification. In the absence of such supercoolings, the rate of external heat extraction limits achievable solid/liquid interfacial velocities to below that required for partitionless solidification [2,5].

Figure 4 shows the proposed solidification "path" of the droplet with no discernible segregation shown in Figure 2(a). First, the thermodynamic restriction on partitionless solidification is denoted by the $T_o^{L/\alpha}$ curve on the binary phase diagram. Partitionless solidification of a crystalline solid can only occur while interfacial temperatures are below this curve. On the other hand, kinetic considerations require interfacial velocities in excess of the diffusive velocity of the solute in the liquid. It has been shown that velocities in excess of several meters per second are possible

if the droplet supercools to a sufficiently low temperature prior to nucleation [1]. The nucleation temperature, T_N, required for the complete partitionless solidification of a powder particle such as the one shown in Figure 2(a), has been defined by the following equation [1]:

$$\int_{T_N}^{T_C} C_p dT > \Delta H_M \qquad (1)$$

where

T_c = some critical temperature below $T_o^{L/\alpha}$

T_N = supercooling temperature at nucleation

C_p = specific heat of the alloy in the liquid state

ΔH_M = latent heat of fusion

The supercooling necessary for a particle to reach the hypercooled condition can be calculated using the following equation.

$$\Delta T_{HYP} = T_l - T_N$$

where

T_l = the equilibrium liquidus temperature

T_N = the nucleation temperature necessary to satisfy Equation (1).

The solidification "path" is then that depicted by the arrows in Figure 4. After nucleation the evolving heat of fusion increases the interfacial temperature. The growth velocity, while decreasing with rising interfacial temperature, remains fast enough to avoid solute partitioning even at the end of solidification at T_C.

Figure 5 shows the phase diagram and the postulated solidification path of the powder particle with a mixed mode of solidification shown in Figure 2(b). The lower region of the powder underwent partitionless solidification while both interface temperature and average droplet

temperature recalesced to T_R along the vertical "path" shown. Solute rejected ahead of the interface resulted in morphological instability and in the cellular solidification noted in the upper portion of the powder particle.

ΔT_{HYP} was calculated using recently derived thermodynamic data for $T_o^{L/\alpha}$, C_p and ΔH_M [6], and Equation (1) above for the alloys used in this study. The results are shown in the following table.

TABLE 1. Effect of Composition on ΔT_{HYP}, T_o and observed particle size at the partitionless to cellular growth transition.

Alloy, wt% Cu	Observed Particle Size At Transition μm	Calculated $T_o^{L/\alpha}$, °C	Calculated ΔT_{HYP}, °C
0.5	>1.1	657	339
1.0	>1.1	653	343
2.0	>1.05	647	345
3.0	>0.55 <1.1	640	347.5
4.5	0.49	631	348
6.0	0.47	621.5	354
10.0	0.24	598	363
15.0	0.22	573	367
20.0	0.20	550.5	361

As the particles decreased in size their cooling rates increased and their probability of harboring nucleating agents decreased [7]. Both effects could be responsible for producing the deeper degrees of supercooling and the resulting hypercooled structures seen in the smallest particles of

each alloy studied. It should also be noted that while partitionless solidification is limited by the $T_o^{L/\alpha}$ temperature, ΔT_{HYP} is measured from T_l. The computation of ΔT_{HYP} is, therefore, a function of T_l, $T_o^{L/\alpha}$, Cp and ΔH_m and is not necessarily a simple monotonically increasing function of C_o. A further complication is the possible nucleation of more than one stable or metastable phases. For this analysis, the nucleation of the FCC Al-Cu phase is the only one considered. As can be seen in Table 1, ΔT_{HYP} increases with composition up to 15 wt% Cu and then decreases. It is therefore possible that an increase in the solute concentration could lead to partitionless solidification under conditions where a lower concentration would not.

Acknowledgement

This work was sponsored by the Defense Advanced Research Projects Agency.

References

1. Levi, C. G. and Mehrabian, R., Met. Trans., 13A, 1982, p. 13.

2. Cohen, M. and Mehrabian, R., Proceedings, Third Conference on Rapid Solidification Processing, NBS, Dec. 1982, p. 1.

3. Shechtman, D., Ridder, S. D. and Mehrabian, R., Proceedings, Third Conference on Rapid Solidification Processing, NBS, Dec. 1982, p. 96.

4. Coriell, S. R., and Sekerka, R. F., Proceedings, Second International Conference on Rapid Solidification Processing, Reston, VA, March 1980, p. 35.

5. Mehrabian, R. International Metals Review, 27, 1982, p. 185.

6. Murray, J. L., Private Communication, NBS, Metallurgy Division, Washington, D.C. 20234, 1984.

7. Perepezko, J. H., Proceedings, Second International Conference on Rapid Solidification Processing, Reston, VA, March, 1980, p. 56.

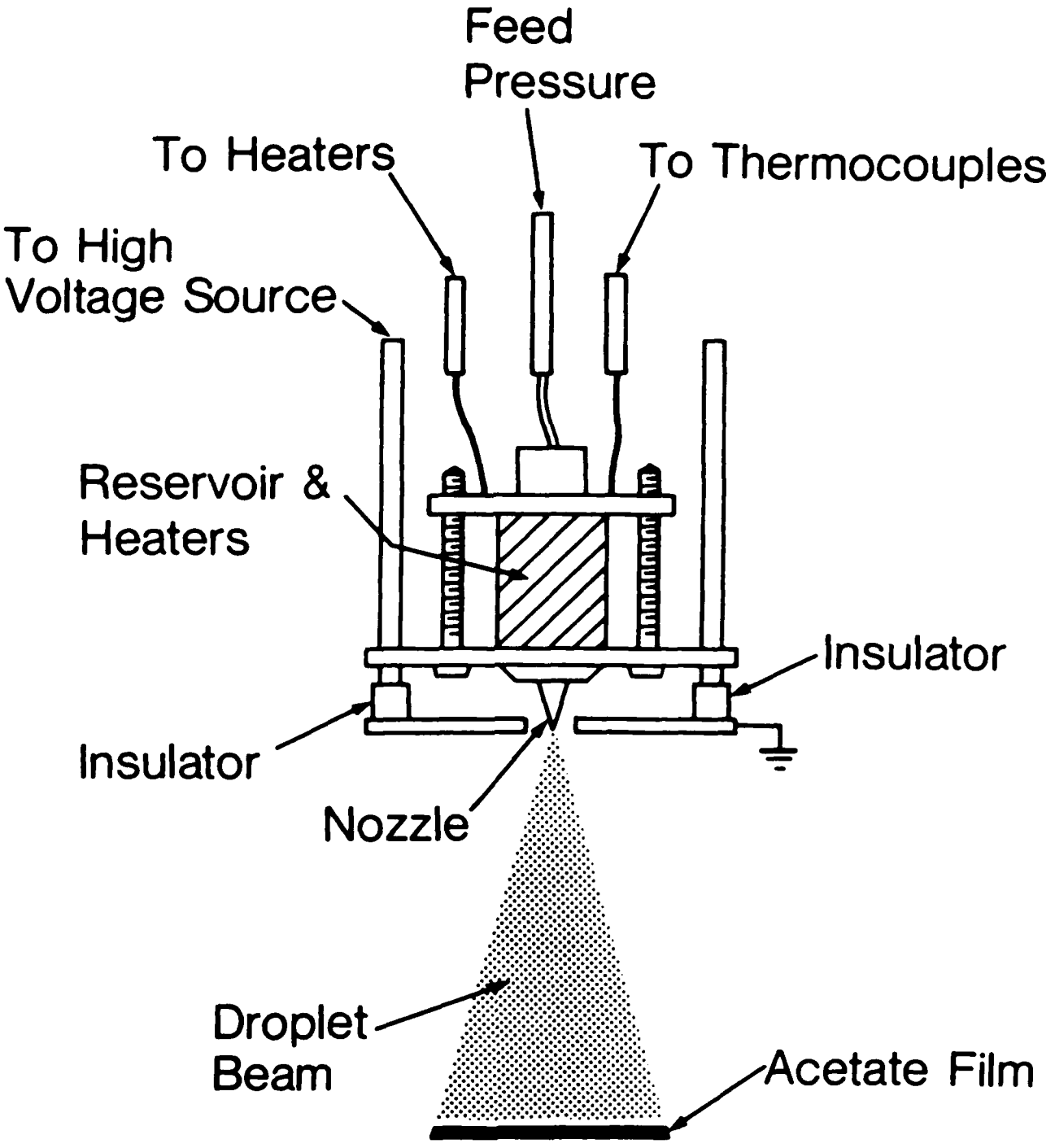

FIGURE 1. Schematic of EHD atomizer.

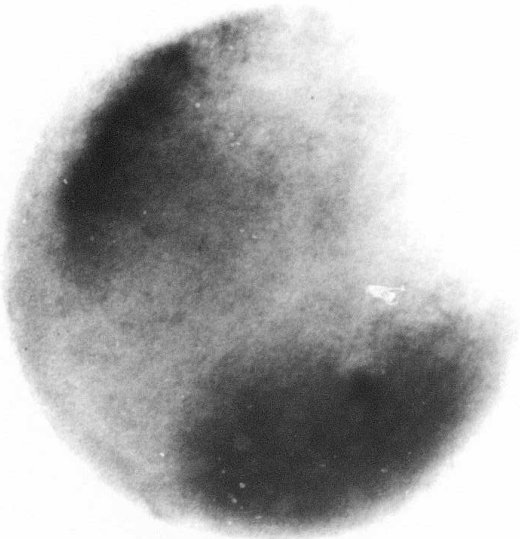

FIGURE 2a. Typical microstructure observed in Al-Cu particles produced by EHD atomization. Segregation-free Al-10 wt% Cu particle 0.22 μm in diameter.

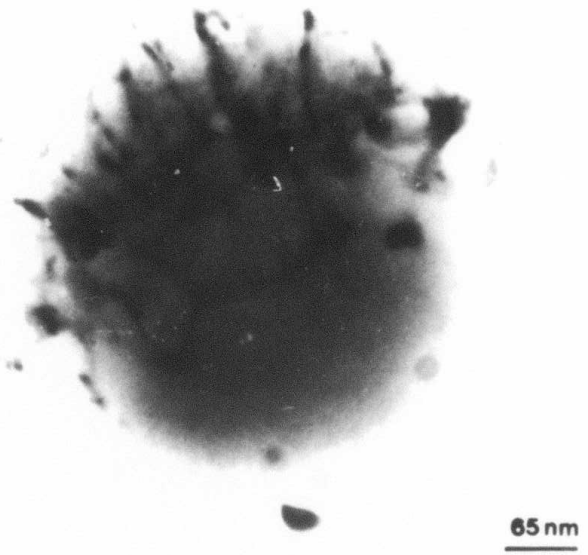

FIGURE 2b. Typical microstructure observed in Al-Cu particles produced by EHD atomization. Mixed mode solidification in an Al-10 wt% Cu particle 0.57 μm in diameter.

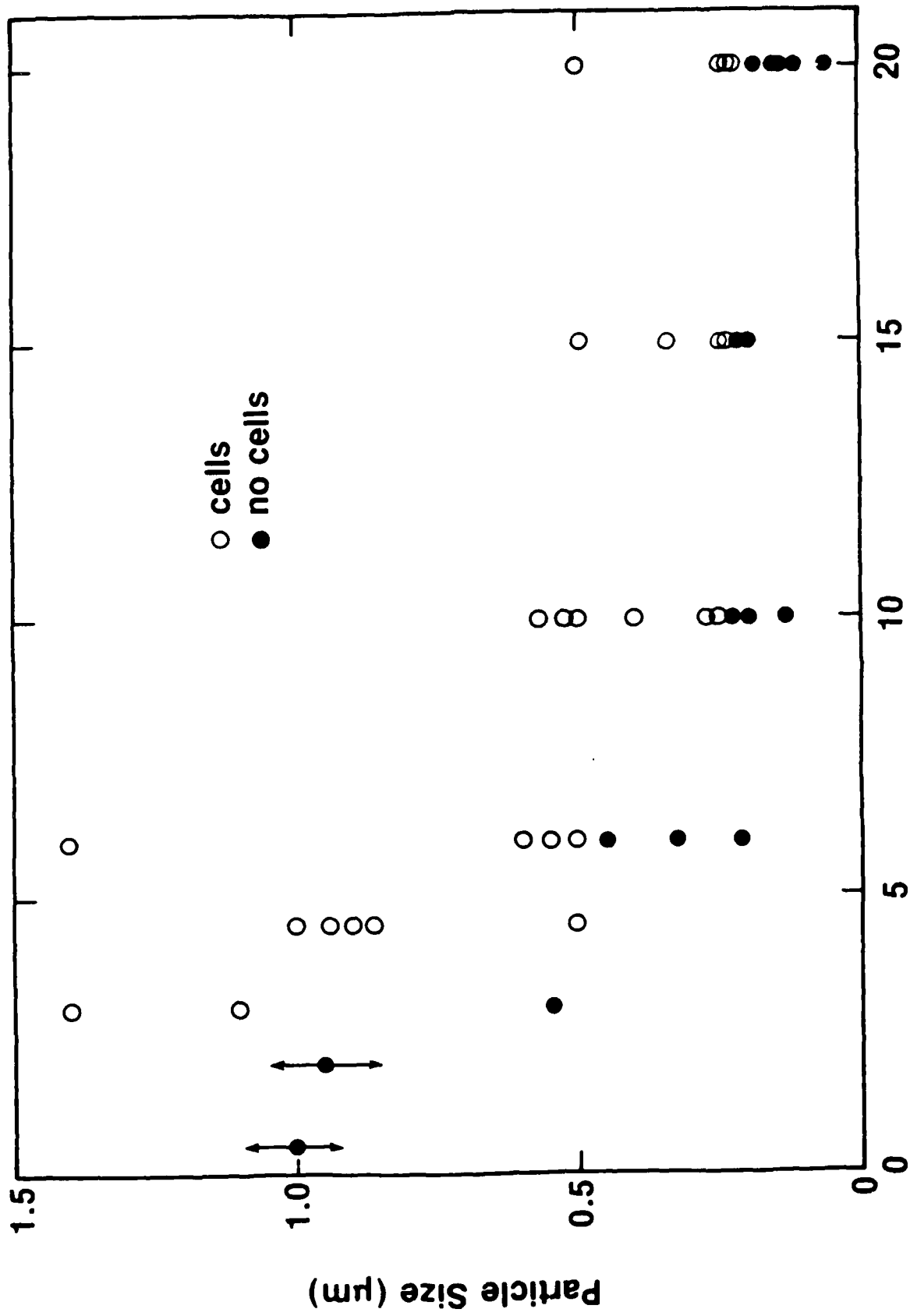

FIGURE 3. Results of microstructural study of Al-Cu particles indicating size, composition and microstructural type observed.

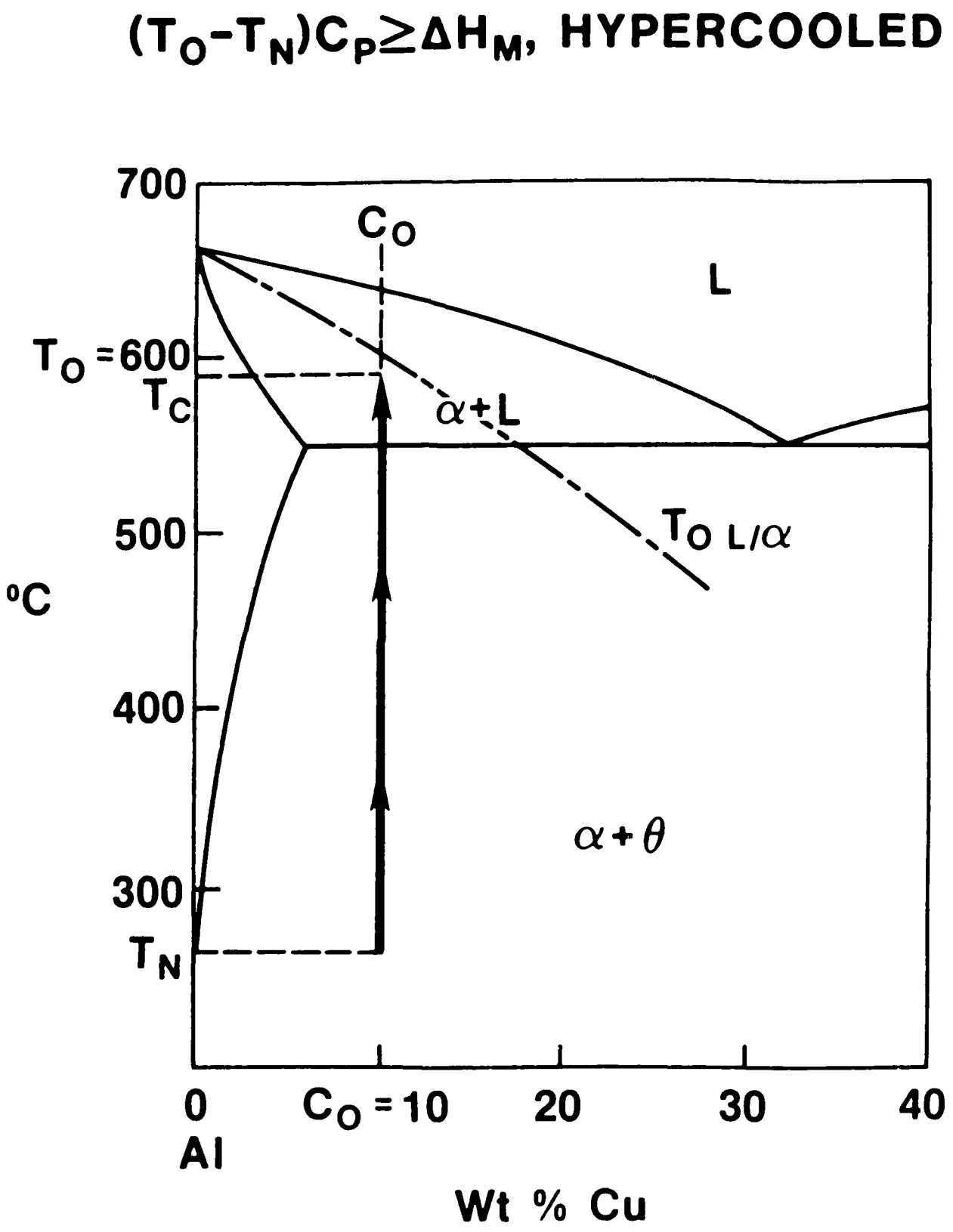

FIGURE 4. Schematic phase diagram of the Al-Cu system showing the solidification path of the rapidly solidified droplet shown in Fig. 2a.

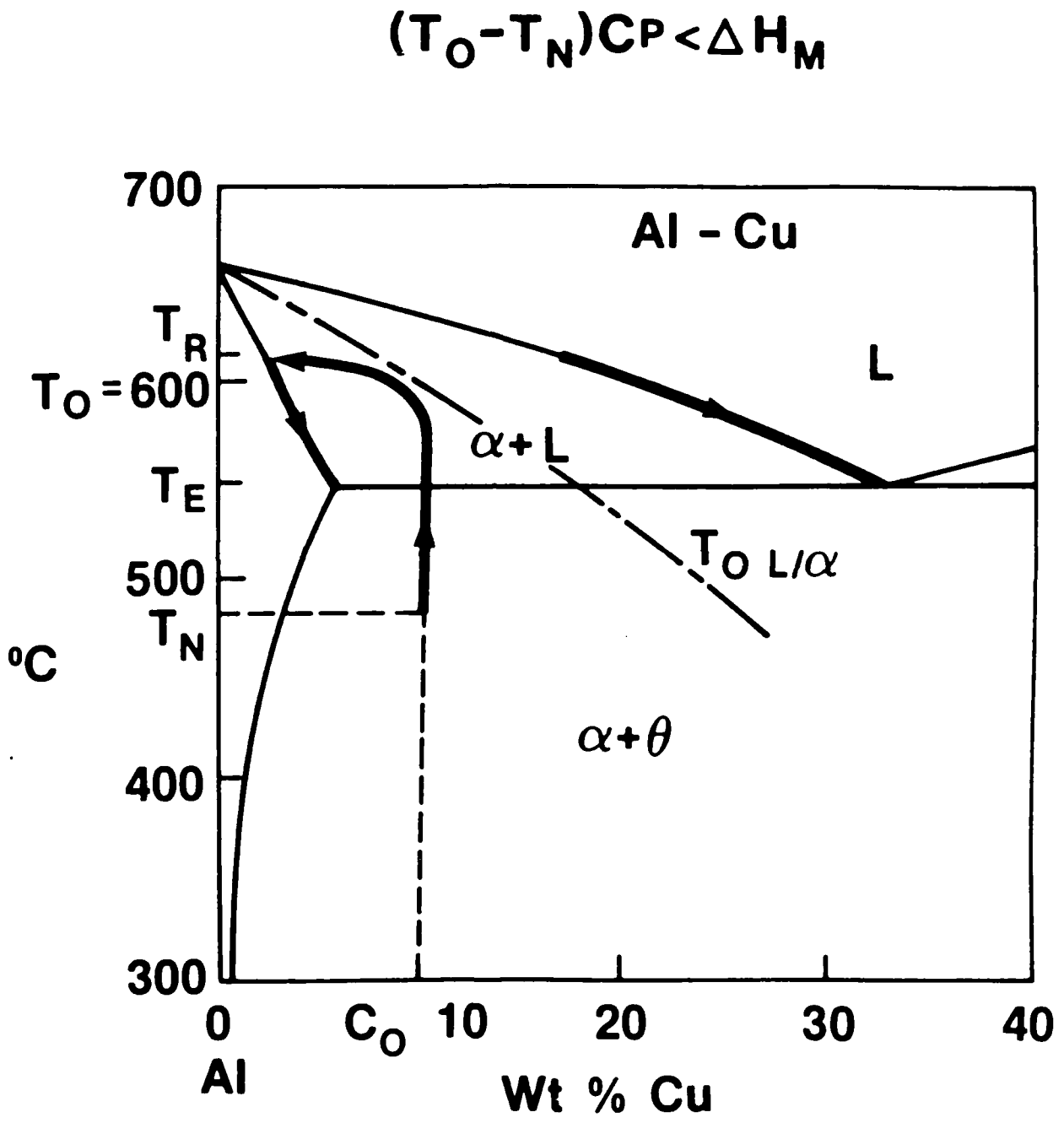

FIGURE 5. Schematic phase diagram of the Al-Cu system showing the solidification path of the droplet shown in Fig. 2b.

THE EFFECT OF RAPID SOLIDIFICATION VELOCITY ON MICROSTRUCTURE AND PHASE SOLUBILITY EXTENSION IN Ni-Aℓ QUASIBINARY EUTECTIC

W. J. BOETTINGER,* D. SHECHTMAN,**

T. Z. KATTAMIS*** AND R. J. SCHAEFFER*

*Metallurgy Division, National Bureau of Standards
Washington, D. C. 20234

**Technion, Haifa, Israel and Center for Materials Research
Johns Hopkins University, Baltimore, Md. 21218

***University of Connecticut, Storrs, Ct.

Published in the Proceedings of the 5th Conference on "Rapid Quenching and Solidificacion of Metals," Eds. S. Steeb and H. Warlimont, September 3-7, 1984.

ABSTRACT

The transition from a two-phase rod-type eutectic microstructure to a single-phase Cr-supersaturated NiAℓ-Cr quasibinary eutectic composition is determined as a function of growth rate by electron beam melting and solidification scans. At growth rates below 1 cm/s the alloy exhibits a two-phase eutectic structure. Above 2.5 cm/s the structure solidifies as single phase Cr-supersaturated NiAℓ which subsequently decomposes spinodally.

1. INTRODUCTION

The NiAℓ-Cr quasibinary eutectic composition is Ni-33 at% Aℓ-34 at% Cr and is of interest for the study of extended solubility because of the similarity of crystal structures (CsCℓ for β-NiAℓ and BCC for α-Cr) and lattice parameters of the two phases in the eutectic.[1] Previous work[2] has shown that melt spun ribbons exhibit a variety of microstructures: extremely fine eutectic, supersaturated β-NiAℓ phase (which undergoes solid state decomposition) and a mixture of the two. The thermodynamic possibility of solubility extension of the two phases was evaluated using T_o curves and was found to be consistent with the formation of supersaturated β-NiAℓ rather than α-Cr from eutectic melts.

The present work seeks to establish the kinetic aspects of the transition from eutectic growth at low solidification rates to be supersaturated single phase structure observed in melt spun ribbons. By careful microstructural analysis of the shape of molten pools during electron beam surface scans performed at speeds between 0.1 cm/s and 50 cm/s, the local growth rate

within solidified zones is determined and correlated to the local microstructure obtained by TEM.

2. EXPERIMENTAL PROCEDURE

Rapidly solidified samples were prepared using one dimensional scans of a focussed electron beam across the surface of the alloy.[3] These scans produce a melted and resolidified trail, typically 0.5mm wide and 0.1 mm deep. Due to the relatively poor thermal diffusivity of the alloy, the growth direction, even at the top center of the trail, differs significantly from the scan direction. Under steady state conditions, the true growth rate, V, is the product of the scan velocity with the cosine of the angle between the growth direction and the scan direction. For scan speeds below 2.5 cm/s these angles were measured for each specimen by longitudinal sections through the trail centerline and were typically 30°. The measured angles were employed to describe the growth rate for the microstructures. For scan speeds above 2.5 cm/s the angles were not measured but are estimated to be about 60° leading to a 50% reduction of the actual growth rate compared to the scan rate. TEM specimens were prepared by ion milling full disks cut parallel to the surface of the alloy or half disks cut perpendicular to the scan direction. In all cases care was taken to locate the thin area near the top center of the melted trail where the growth rate is known from the above arguments.

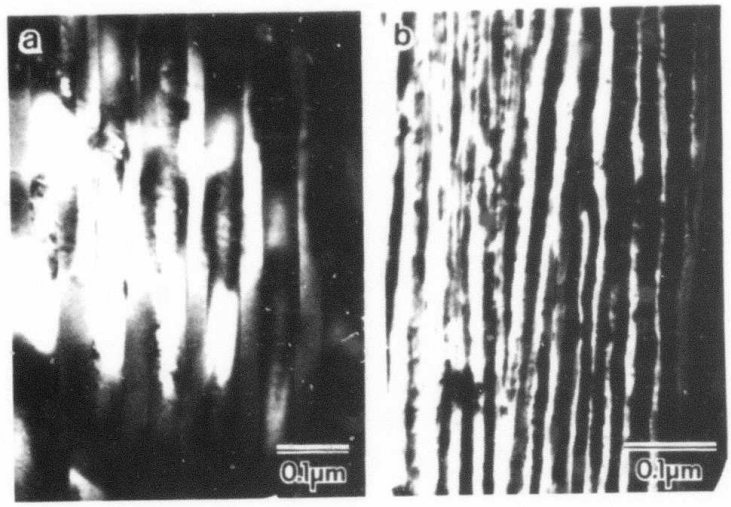

FIGURE 1. Eutectic structures of α-Cr and β-NiAℓ solidified at (a) 0.09 cm/s and (b) 0.8 cm/s with spacings of ∿ 80 nm and ∿ 20 nm respectively. TEM.

3. RESULTS

For growth rates below 1 cm/s the alloy solidifies as a fine eutectic structure of β-NiAℓ and α-Cr phases as shown in Fig. 1. The observed eutectic spacings, λ_e, are plotted on the left side of Fig. 4 along with an extrapolation of the relationship between spacing and growth rate determined at slower rates by Walter and Cline.[4] ($\lambda_e^2 V = 7 \times 10^{-12}$ cm^3/s For eutectic growth at rates on the order of 1-10 cm/s, the interfacial undercooling due to solute redistribution and interface curvature becomes sufficiently large that the temperature dependence of the liquid diffusion becomes important.[3] Hence the $\lambda_e^2 V$ relationship cannot be extrapolated past this range. In fact, in the present case at a growth rate of 2.5 cm/s and above, the alloy does not solidify as with a eutectic structure.

Fig. 2a shows the microstructure obtained at 2.5 cm/s. It consists of columnar grains of β-NiAℓ which have undergone spinodal decomposition. The average composition appears quite uniform across the grain interiors as judged by the uniformity of the decomposition structure across the grains. Antiphase domains (not shown) are present within the grains with sizes which are very large compared to the scale of the spinodal structure. This fact indicates that the structure was ordered before it decomposed and consequently that the supersaturated β-NiAℓ formed directly from the melt. Identical structures were obtained in melt-spun ribbons.[2]

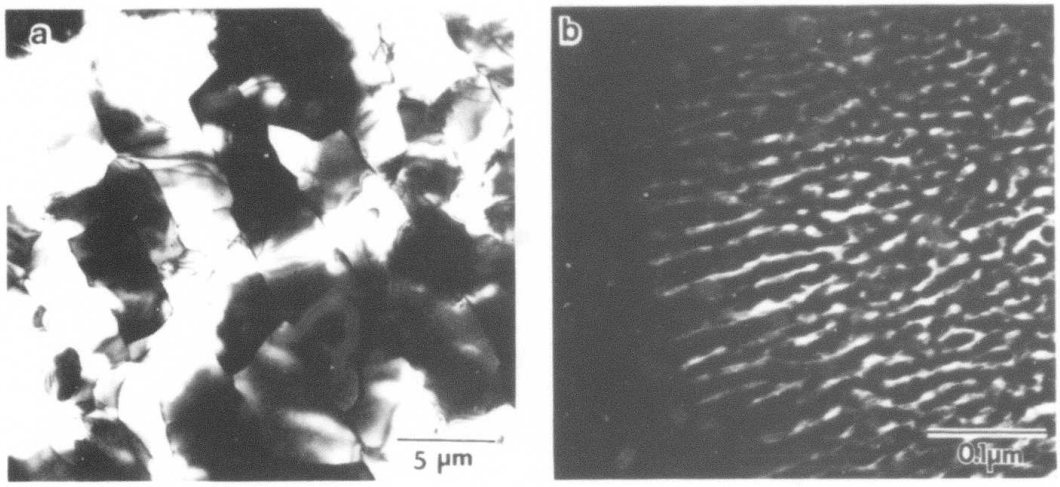

FIGURE 2. (a) Columnar grains of supersaturated β-NiAℓ produced at 2.5 cm/s (oblique section).

(b) Fine structure of decomposed supersaturated β-NiAℓ. TEM.

A high magnification view of the nature of the region near a grain boundary is shown in Fig. 2b. On the right is seen the spinodal structure present throughout the grains. The structure shows no direction of elongation regardless of the plane of section and therefore is not eutectic. On the left, close to the edge of the grain, a fine structure aligned perpendicular to the boundary is present. Even though this resembles a fine eutectic, it is thought to arise in the solid state by a peculiarity of coarsening of the spinodal structure near a grain boundary.[5] In melt spun ribbons,[2] similar structures were observed but also intergranular regions which were clearly composed of eutectic. This latter structure was not seen in the electron beam melted specimens, possibly due to the absence of recalescence effects in surface melted specimens.

The general features of the microstructure do not vary significantly at increased growth rates (see Fig. 3) except that the spinodal spacing decreases with increasing growth rate. These spacings are shown on the right side of Fig. 4.

4. DISCUSSION

Three topics warrant discussion in the present paper: (1) the existence of a maximum growth rate of $\sim$ 1-2 cm/s for the α-Cr and β-NiAl eutectic; (2) the formation of the supersaturated β-NiAl phase at the relatively low growth rates of 2.5 cm/s and above; and (3) the refinement of the spinodal spacing with increasing growth rate.

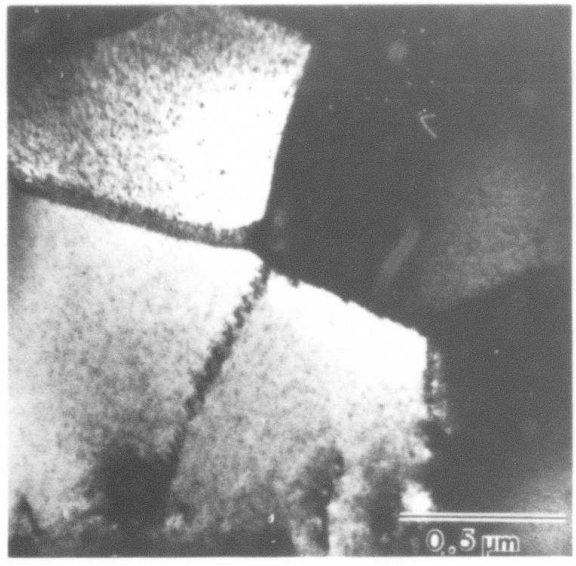

FIGURE 3. Transverse section of columnar grains of supersaturated β-NiAℓ produced at 50 cm/s showing pairs of dislocations in the ordered structure at a low angle grain boundary. TEM.

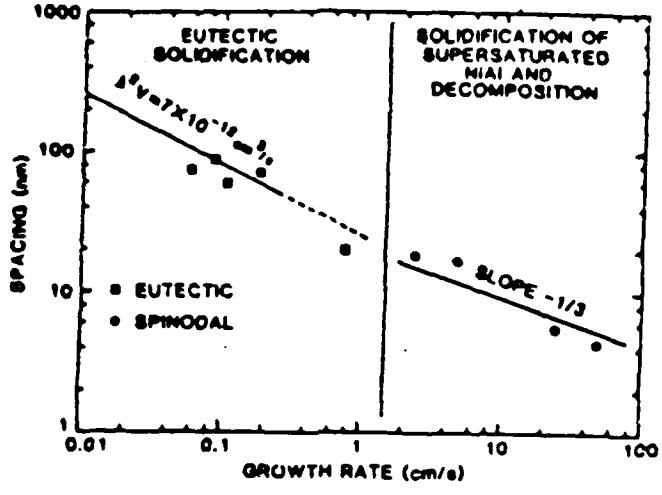

FIGURE 4. Eutectic spacing observed at low velocity and spinodal spacing in decomposed supersaturated β-NiAℓ observed at high velocity as a function of growth rate.

4.1 Eutectic Growth Rate Maximum

The observed growth rate maximum for the eutectic structure is consistent with theoretical arguments and results on other systems.[3] Inclusion of the temperature dependence of the liquid diffusion coefficient into eutectic growth theory predicts a maximum growth rate in the range of 1-10 cm/s for most eutectics. This modification of the theory also leads to a modification of the $\lambda_e^2 V$ relationship obtained at slow rate. However this modification only becomes detectable experimentally very close to the growth rate maximum. This fact is reflected in the present work by the good agreement of the measured eutectic spacings with the extrapolated $\lambda_e^2 V$ relation of Cline and Walter. Presumably measurements of spacings between 1 and 2.5 cm/s would show a marked deviation from the extrapolated $\lambda_e^2 V$ relationship.

4.2 Supersaturated β-NiAℓ

As described previously,[2] the formation of β-NiAℓ by partitionless solidification from liquid of eutectic composition is thermodynamically favored over the formation of α-Cr. This conclusion is based on an analysis of the T_o curves of the NiAℓ-Cr quasibinary system. Partitionless solidification not only requires interface undercooling below the T_o curve but also growth at sufficiently high rates to cause solute trapping. For dilute alloys, this rate is thought to be near or less than the ratio of the liquid diffusion coefficient to the interatomic dimensions or about 5 m/s for most metallic systems. Therefore, the formation

of the supersaturated β-NiAℓ structure at growth rates as low as 2.5 cm/s in the present work is quite surprising. One possible reason for this result lies in the fact that the velocity required for partitionless solidification in concentrated alloys may be smaller than that required for dilute alloys.[6-7] Such a trend was seen in Ag-Cu alloys where a growth rate of 0.7 m/s (compared to 5 m/s) was required for alloys of eutectic composition.[3] Another explanation for this result could lie in the fact that partitionless solidification has not occurred. Planar growth with equilibrium partitioning with solid forming at the metastably extended solidus curve can produce microsegregation-free solids.[6] The published phase diagram data[8] is sparse but would be inconsistent with this second possibility. Future analysis of this result is necessary.

4.3 Spinodal Spacing

For the case of a moving heat source the average cooling rate in the solid behind the freezing interface can be estimated as being proportional to the source speed, V. For the case of continuous cooling the spinodal spacing, λ_s, should vary as a power of the solid cooling rate.[9] For the present case where extensive coarsening has taken place the power is roughly -1/3[5] and hence $\lambda_s \sim V^{-1/3}$. The variation of spinodal spacing with electron beam scan rate in Fig. 4 is not inconsistent with this relationship.

REFERENCES

1. J. L. Walter, H. E. Cline and E. F. Koch, Trans. TMS-AIME 245 (1969) 2073.

2. D. Shechtman, W. J. Boettinger, T. Z. Kattamis, and F. S. Biancaniello, Acta Met. 32 (1984) 749.

3. W. J. Boettinger, D. Shechtman, R. J. Schaefer and F. S. Biancaniello, Met. Trans 15A (1984) 55.

4. J. L. Walter and H. E. Cline, Metall. Trans. 1, (1970) 1221.

5. J. W. Cahn, private communication.

6. W. J. Boettinger, S. R. Coriell and R. F. Sekerka, Mat. Sci. & Eng. (1984).

7. M. J. Aziz, Appl. Phys. Lett. 43 (1983) 552.

8. I. I. Kornilov and R. C. Mintz, Kokl. Akad. Nauk. USSR 94, (1954) 1085.

9. E. I. Huston, J. W. Cahn and J. E. Hilliard, Acta Met. 14 (1966) 1053.

CELLULAR MICROSEGREGATION IN RAPIDLY SOLIDIFIED Ag-15 wt% Cu ALLOYS

L. A. BENDERSKY* AND W. J. BOETTINGER**

*Center for Materials Research, Johns Hopkins University, Baltimore, Maryland 21218

Guest worker, Metallurgy Division, National Bureau of Standards

**Metallurgy Division, National Bureau of Standards, Washington, D. C. 20234

Published in the Proceedings of the 5th Conference on "Rapid Quenching and Solidifiecation of Metals," Eds. S. Steeb and H. Warlimont, September 3-7, 1984.

ABSTRACT

Microstructural and microchemical analysis has been performed on Ag-15 wt% Cu alloys produced by electron beam melting with solidification velocities of 2.5, 12 and 18 cm/s. Cellular structures of the Ag-rich phase are produced with spacings of 0.8, 0.3 and 0.2μm, respectively. Intercellular regions contained fine eutectic at the lowest speed but only Cu-rich phase at the higher speeds. The composition within the cells was found to be nearly uniform and 12.5 ± 1 wt% Cu. The uniformity and level of the Cu content within the cells are discussed.

1. INTRODUCTION

Many rapidly solidified crystalline alloys exhibit very fine cellular microsegregation patterns. The amount of solute incorporated into the cell interiors has a strong influence on the volume fraction of intercellular phases and precipitation in the cell interiors during subsequent thermomechanical treatment. At extremely high rates of solidification (∿1 m/s), microsegregation-free alloys may be produced by solute trapping.[1] However, many important rapid solidification processes do not impose such high growth rates. Hence the details of microsegregation patterns were examined at lower growth rates where significant solute trapping is not expected.

Several authors have measured cellular solute profiles in rapidly solidified alloys produced with unknown or calculated growth rates.[2-5] In the present work the growth rate is determined experimentally using the electron beam melting and resolidification technique.[6]

The theory of alloy dendritic and/or cellular growth under conditions of local interfacial equilibrium is being continually refined.[7-8] Solari and Biloni,[9] using the model of Burden and Hunt[10] for the tip concentration, have modeled the entire microsegregation profile as a function of growth rate under the assumption of no lateral concentration gradients in the liquid between solidifying cells. Such an approach is only valid when the cell spacing, λ_1, is much less than D/V, where D is the liquid diffusion coefficient and V is the growth rate. As will be shown in the present paper, this assumption is questionable for rapid solidification.

2. EXPERIMENTAL PROCEDURE

Rapidly solidified samples were prepared using one dimensional scans of a focussed electron beam across the surface of a Ag-15 wt% Cu sample at speeds of 2.5, 12, and 18 cm/s. Due to the relatively high thermal diffusivity of Ag, the growth direction and solidification speed of the resolidified alloy near the top center of the melted region is nearly parallel and equal to the electron beam scan velocity. TEM samples were prepared by ion milling on a liquid nitrogen cooled stage (thin half disks cut transverse to the scan direction).

Composition profiles were determined using analytical electron microscopy. Compositions were quantified using the Cliff-Lorimer ratio technique[11] for the L_α and K_α x-rays for Ag and Cu with a constant determined experimentally from measurements on a homogeneous Ag-28 wt% Cu alloy, rapidly solidified in a

partitionless manner at a velocity of 70 cm/sec.[6] The thin-film criterion[11] is satisfied for a specimen thickness less than 153 nm for both characteristic x-rays. The usual thickness of specimens was less than 150 nm. The spatial resolution was determined using the beam broadening equation.[11] For the foil thickness, 150 nm, the beam broadening was calculated to be 42 nm, and the total broadening with the probe size 5 nm (in our experiments) was 42.2 nm.

3. RESULTS AND DISCUSSION

3.1 Microstructure

Figure 1 shows micrographs of cellular structures of Ag-rich phase seen in Ag-15 wt% Cu alloys solidified at 2.5, 12, and 18 cm/s. The distance between cells are approximately 0.8, 0.3, and 0.2 μm respectively. Note that these values when divided by D/V, the characteristic diffusion length, are in excess of 10. (D is taken as 2×10^{-5} cm^2/s).

The volume fraction of intercellular regions is small compared to that found in conventionally cast alloy of the same composition. This is due to the high level of solute present in the cell interiors (see Section 3.2). At a growth rate of 2.5 cm/s (Fig. 1a), those intercellular regions which are wide, contain a fine eutectic structure of the Ag- and Cu-rich phases. The eutectic spacing is ∿48 nm. In narrow intercellular regions, only the Cu-rich phase is seen. This feature, which also occurs in ordinary cast microstructures, is called a divorced eutectic and is present whenever the width of an intercellular region is

smaller than the eutectic spacing which would occur at the imposed growth rate.

Figure 2 shows a high magnification micrograph of intercellular regions typical of those seen at 12 and 18 cm/s. No eutectic is seen at these growth rates. The intercellular regions are comprised solely of the Cu-rich phase (fringe pattern). This divorced eutectic occurs for a different reason at high growth rates. It is known that the Ag-Cu eutectic cannot grow faster than 2.5 cm/s.[6] Hence the eutectic should also be absent as an intercellular microconstituent at growth rates higher than 2.5 cm/s.

3.2 Microanalysis

Figure 3 shows a STEM micrograph and an associated microanalysis profile of the relatively coarse cellular structure formed at 2.5 cm/s. Typical spatial and composition resolutions are 40 nm and 2 wt% Cu. Within these limitations, the composition of the cell interiors is uniform with 11.8 ± 1.3 wt% Cu. The measured compositions in the cell walls are lower than the true composition due to the beam broadening and the fact that the cell wall is slightly oblique to the electron beam with Ag-rich phase also being probed. In regions of the foil where the Ag-rich phase has been completely removed by ion milling, the composition of the Cu-rich intercellular phase was found to be ∿90 wt% Cu.

A similar profile for finer cells grown at 12 cm/s is shown in Figure 4. The cell interior is uniform with 12.3 ± 1.2 wt% Cu. The center composition of a number of the very fine cells produced at 18 cm/s were measured as shown in Figure 5. The average of these measurements was 13.6 ± 1.6 wt% Cu.

Two aspects of these profiles warrant discussion: the uniformity of the compositions within the cells and the level of solute within the cells. The slight increase in cell compositions from 11.8 to 13.6 wt% Cu with increasing growth rate cannot be documented with certainty in the present work and the solute level of all the cells will be taken as ∿12.5 wt% Cu.

At growth rates used in the present work, the assumption of local interfacial equilibrium at the liquid/solid interface should be valid[1] and, in fact, partitionless solidification is only observed in Ag-15% Cu at growth rates above 2 m/s.[7] Hence the phase diagram is of interest. Recently Murray[12] included in her assessment an evaluation of the free energy of the phases which permits the calculation of the metastable Ag-rich solidus below the eutectic temperature. The solidus has a metastable retrograde at 10.5 wt% Cu and 700°C. Under interfacial equilibrium conditions solid cannot form with composition higher than the retrograde composition. The observed level of solute in the cells is very close to the retrograde composition. The agreement may be even better considering the fact that minor adjustments of the free energy functions can increase this retrograde composition by a few percent.[13]

The observation of uniform compositions across cell interiors but with a high degree of segregation to the cell walls is a seemingly curious result. Mazur and Flemings[2] in work on Aℓ-Cu did not see uniformity within cell interiors. However the spacings of the cells measured in their work were greater than 2 μm whereas the cells measured in the present work are less than 1 μm.

The theory of Solari and Biloni,[9] while predicting a reduced level of microsegregation at high growth rates, does not predict uniform profiles within cell interiors. This is due to their assumption which does not allow lateral solute gradients. Non-equilibrium trapping of solute is often used as an explanation of flat microsegregation profiles. However, McFadden and Coriell[14] have numerically calculated solute concentrations, temperature fields and interface shapes for two-dimensional cellular interfaces in a self-consistent manner. They have shown that compositions may be quite uniform across the major fraction of a cell with strong segregation to cell walls even when local equilibrium exists at the liquid-solid interface. Such microsegregation profiles should be very commen whenever $10 < \frac{\lambda_1 V}{D} < 100$. Such is the case in the present experiments.

ACKNOWLEDGEMENT

The authors wish to thank S. R. Coriell, G. B. McFadden and R. J. Schaefer for many helpful discussions.

REFERENCES

1. W. J. Boettinger, S. R. Coriell, and R. F. Sekerka, Mat. Sci. & Eng., 65 (1984), 27.

2. L. J. Mazur and M. C. Flemings, Proc. 4th Int. Conf. on Rapidly Quenched Metals, Vol. 2, T. Mazumoto, Suzuki, eds., Japan Inst. of Metals, Sendai (1982), 1557.

3. T. Z. Kattamis and R. Mehrabian, J. Mat. Sci. 9 (1974) 1446.

4. T. F. Kelly, G. B. Olson, and J. B. Vander Sande, in Rapidly Solidified Amorphous and Crystalline Alloys, B. H. Kear, B. C. Giessen, and M. Cohen eds., North Holland, 1982, 343.

5. H. Palacio, M. Solari, and H. Biloni in Physical Metallurgy, Part 1 ed. by R. W. Cahn and P. Haasen, North Holland, Amsterdam (1983), 526.

6. W. J. Boettinger, D. Shechtman, R. J. Schaefer, F. S. Biancaniello, Met. Trans., 15A, 55, 1984.

7. R. Trivedi, J. Cryst. Growth 49, (1980), 219.

8. W. Kurz and D. J. Fisher, Acta Met. 29 (1981), 11.

9. M. Solari and H. Biloni, J. Cryst. Growth 49 (1980), 451.

10. M. H. Burden and J. D. Hunt, J. Cryst. Growth 22 (1974), 109.

11. J. I. Goldstein, Introduction to Analytical Electron Microscopy, eds. J. J. Hren, J. I. Goldstein, and D. C. Joy, Plenum Press, NY, 1979, p. 83.

12. J. F. Murray, Met. Trans, 15A (1984), 261.

13. J. F. Murray, private communication.

14. G. B. McFadden and S. R. Coriell, Physica D (1984), in press.

FIGURE 1. Cellular structures in Ag-15 wt% Cu solidified at (a) 2.5 cm/s (dark field), (b) 12 cm/s, and (c) 18 cm/s. TEM.

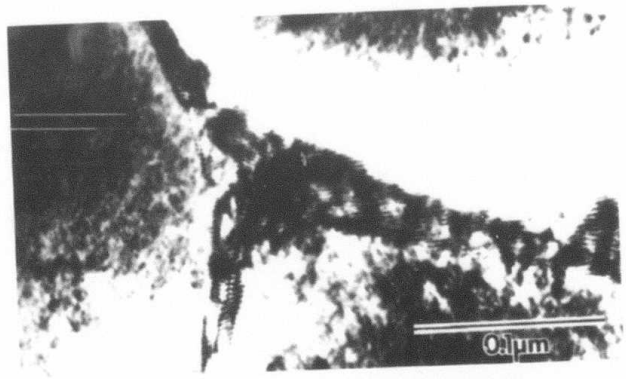

FIGURE 2. Intercellular region in alloy solidified at 12 cm/s. TEM.

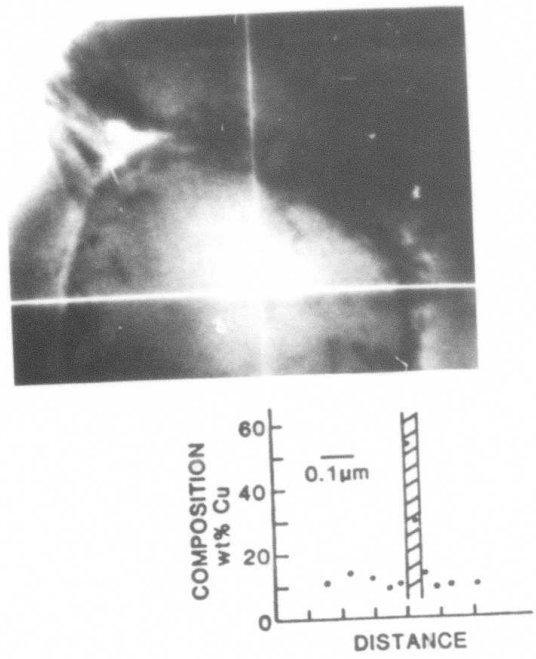

FIGURE 3. STEM micrograph and composition profile across intercellular region of alloy solidified at 2.5 cm/s.

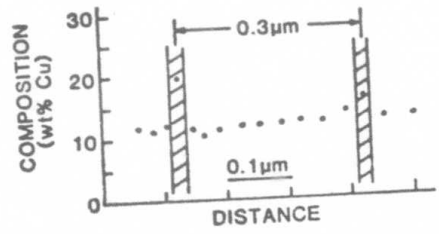

FIGURE 4. Composition profile across a cell solidified at 12 cm/s.

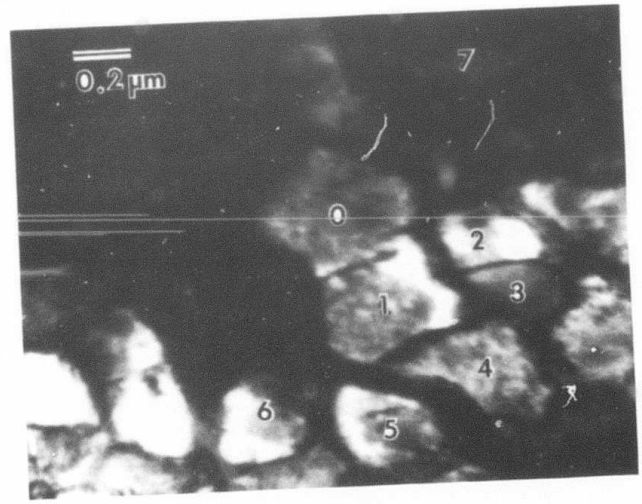

FIGURE 5. STEM micrograph of cellular structure solidified at 18 cm/s. The compositions at the centers of the cells marked 0, 1, ... 7 respectively are 12.5, 13.0, 13.8, 15.5, 14.8, 13.8, 12.0, 13.2 wt% Cu.

ORIENTATION RELATIONSHIP BETWEEN PRECIPITATED $Al_9(Fe,Ni)_2$ PHASE AND α-ALUMINUM

L. BENDERSKY*
Center for Materials Research
The Johns Hopkins University
Baltimore, Maryland 21218

*Guestworker, Metallurgy Division, National Bureau of Standards, Gaithersburg, Maryland 20899

To be published in Metallurgical Transactions.

I. INTRODUCTION

The Al_9Co_2-type phase is of significant interest in aluminum alloy design. The Al_9Co_2 phase has been investigated in unidirectionally solidified Al-Al_9Co_2 eutectic alloys and the orientation relationship, $(100)_{Al_9Co_2}//(001)_{Al}$, determined [1,2]. For more complex alloys (e.g., Al-3.3 Fe-2.3 Ni-4.6 Co in the rapidly solidified condition) different morphologies of the $Al_9(Fe,Ni,Co)_2$ phase were observed, including particles which were elongated parallel to the <100> of the Al matrix [3,4]. Alcoa's RS alloys 7091 and 7090 with cobalt content up to 1.6 wt% show precipitation of fine Al_9Co_2 or $Al_9(Co,Fe)_2$ phase [5]. A phase designated Al_9Fe_2 was found by electron diffraction in the ternary Al-Fe-Si system (Al-0.5 Fe-0.2 Si wt% alloy) to be isomorphous with Al_9Co_2 and was shown to be monoclinic with lattice parameters: a=0.869 nm, b=0.635 nm, c=0.632 nm, β=93.4° [6]. The equilibrium $Al_9(Fe,Ni)_2$ phase exists in the ternary Al-Fe-Ni system over a wide range of stoichiometry [7-10]. X-ray diffraction of this phase, grown in equilibrium at 750°C from the Al rich liquid phase, confirmed $Al_9(Fe,Ni)_2$ to be isomorphous with Al_9Co_2 (monoclinic structure, space group $P2_1/a$) and showed the lattice parameters to be: a=0.8598 nm, b=0.6271 nm, c=0.6207 nm, β=94.660 [11]. The latter phase has been found to exist in different morphologies in a rapidly solidified Al - 3.7 Ni - 1.5 Fe (weight %)

alloy and is expected to offer promising high-temperature mechanical properties due to its apparent thermal stability [12,13].

II. EXPERIMENTAL RESULTS

In the present work, the orientation relationship between $Al_9(Fe,Ni)_2$ precipitates and the FCC aluminum matrix in rapidly solidified Al - 3.2 Ni - 1.5 Fe (wt%) alloy has been determined. The specimens were prepared as ribbons by inert gas melt-spinning. A variety of microstructures was found to exist across the ribbon thickness, depending on the local solidification conditions. This subject is discussed elsewhere [14]. For the present study, the microstructures found near the wheel side of the ribbons were investigated by transmission electron microscopy. Accordingly, TEM specimens were prepared by one sided jet electropolishing in a standard solution of 15% HNO_3 and 5% $HC10_4$ in methanol at -30°C.

The microstructure was found to consist of columnar grains of Al with an uniform distribution of precipitates, approximately 20 nm in size (Fig. 1). The columnar grains are elongated in the growth direction, i.e., normal to the ribbon surface, have the nominal alloy composition and are free of any microsegregation. The observed microstructure is developed in two stages: first, the supersaturated solid solution of α-Al is formed from the melt by partitionless solidification [14,16]; and second, the solid decomposes by precipitation during continuous cooling immediately after solidification. This work, where the many-variant orientation

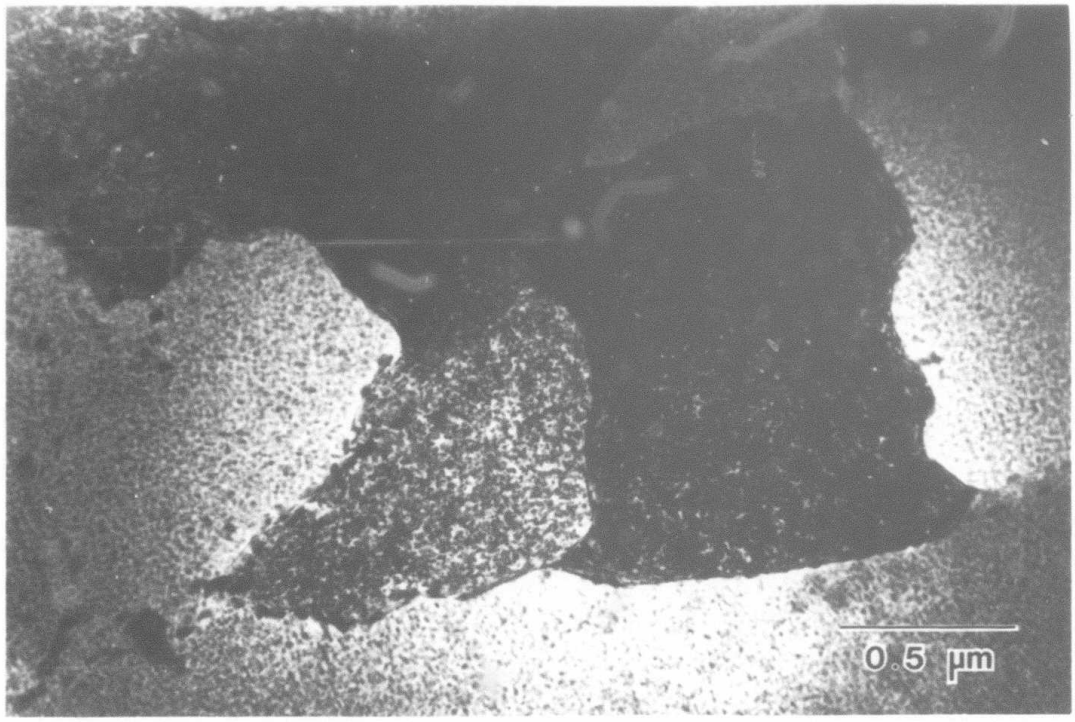

Fig. 1. Columnar grains with uniformly distributed precipitates. TEM, a bright field image.

relationship was found between precipitates and matrix (later discussion), shows the solid state reaction takes place. In the case of a liquid/solid reaction, usually the orientation relationship is mono-variant.

When the TEM specimen is oriented close to the <100> zone axis of the Aℓ matrix, the particles occur as discs lying on {100} planes of the aluminum matrix, as shown in Fig. 2. Diffraction streaks of precipitates, lying in $<100>_{A\ell}$ direction and perpendicular to the disc planes, confirm this. This same geometry was found for precipitates in a rapidly solidified Aℓ-Fe-Co-Ni alloy [4], however, the origin of such particles was unclear.

Selected area diffraction patterns (SADP) from different low-index zones of the aluminum matrix are shown in Fig. 3. The symmetry of the precipitate reflections suggests the existence of an orientation relationship between the precipitates and the matrix with a limited number of orientation variants. However, conclusive identification of the precipitate phase from this pattern is not possible. Nevertheless, by analyzing an SADP tilted slightly away from the axes, a single variant diffraction pattern from the precipitate could be extracted (Fig. 4a). In addition, a single crystal microdiffraction pattern was obtained from the large precipitate (Fig. 4b). As a result, it is possible to conclude that the precipitates are $A\ell_9Co_2$- type $A\ell_9(Fe,Ni)_2$ phase with lattice parameters similar to those obtained in [5] for the $A\ell_9Fe_2$ phase. The

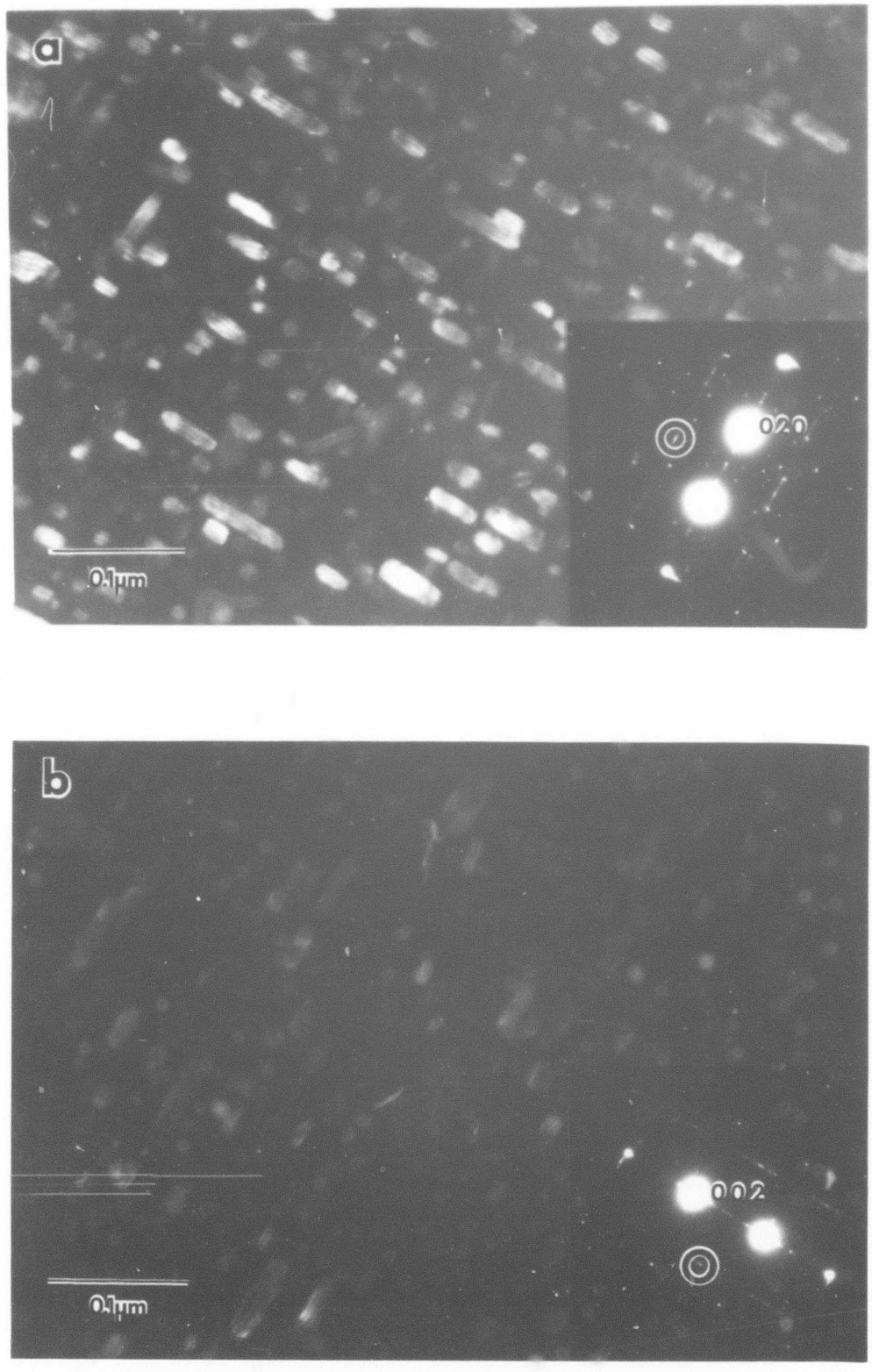

Fig. 2. The orientation of precipitates in a thin foil oriented close to [100] zone axis of aluminum matrix. Disc-like particles are perpendicular to $\langle 100 \rangle_{Al}$ direction and to streaks. a) Dark field image using the circled reflection of precipitates, discs are normal to $[010]_{Al}$; b) the same, discs are normal to $[001]_{Al}$.

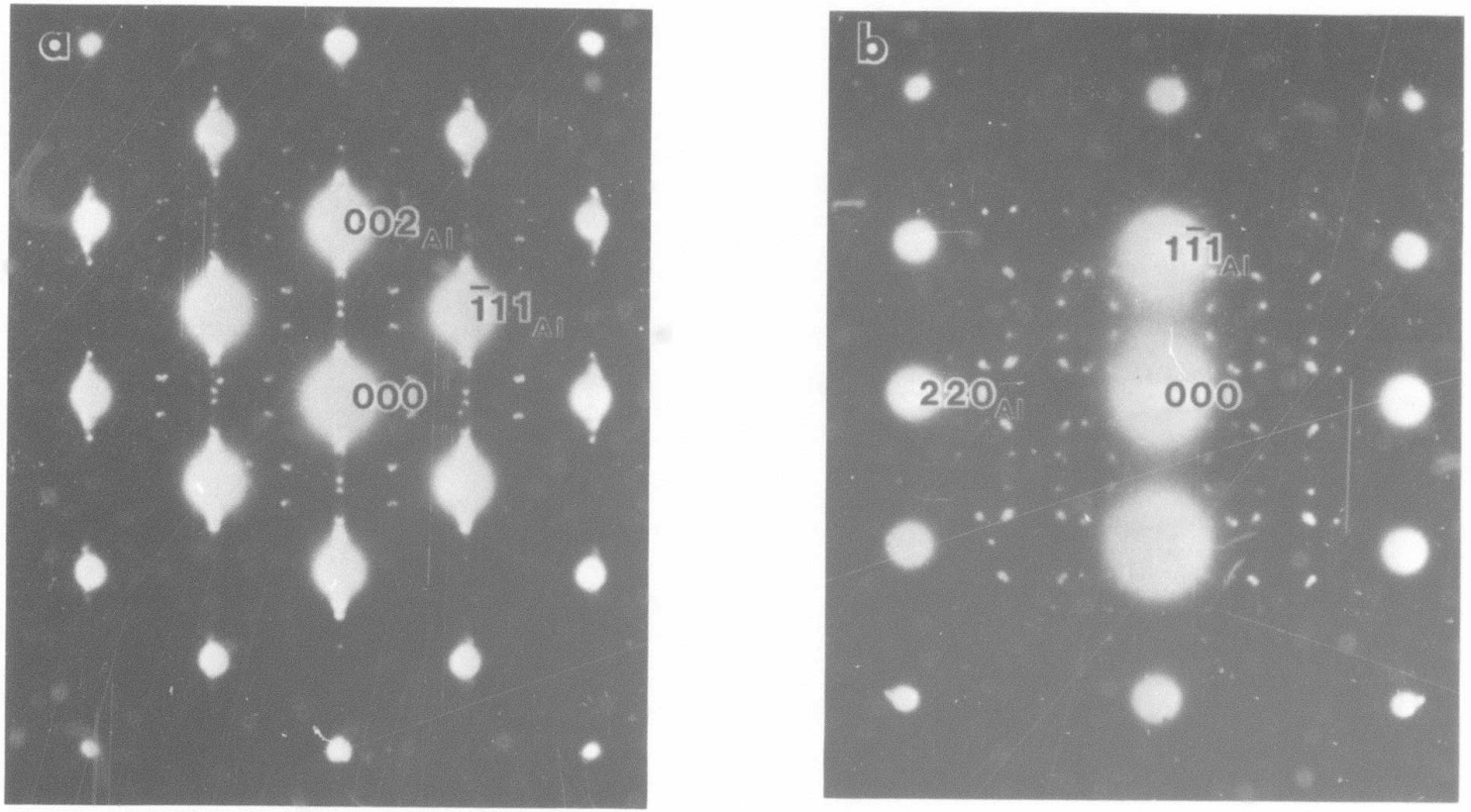

Fig. 3. SADP which show a) $\overline{B}=[110]_{Al}$; b) $\overline{B}=[11\overline{2}]_{Al}$.

orientation relationship obtained from diffraction patterns similar to the one in Fig. 4a is:

$$(\bar{1}11)_{Al} \parallel (2\bar{1}2)_{Al_9(Fe,Ni)_2}$$

$$[\bar{1}12]_{Al} \parallel [\bar{1}22]_{Al_9(Fe,Ni)_2}$$

or

$$(220)_{Al} \parallel (431)_{Al_9(Fe,Ni)_2}$$

Superimposing Al and $Al_9(Fe,Ni)_2$ stereograms yielded a simpler orientation relationship which agreed to within 2°:

$(001)_{Al} \parallel (100)_{Al_9(Fe,Ni)_2}$ $\quad$ $(001)_{Al} \parallel (100)_{Al_9(Fe,Ni)_2}$

$(100)_{Al} \parallel (031)_{Al_9(Fe,Ni)_2}$ or $110_{Al} \parallel [012]_{Al_9(Fe,Ni)_2}$

and

$(100)_{Al} \parallel (013)_{Al_9(Fe,Ni)_2}$

Fig. 5 shows superimposed Al and $Al_9(Fe,Ni)_2$ stereograms for the orientation variant $(001)_{Al}//(100)_{Al_9(Fe,Ni)_2}$ and $(010)_{Al}//(013)_{Al_9}$, also satisfy $(\bar{1}00)_{Al}//(0\bar{3}1)_{Al_9(Fe,Ni)_2}$ relationship.

The proposed orientation relationship is supported by: 1) the relationship $(100)_{Al_9Co_2}//(001)_{Al}$, which was found

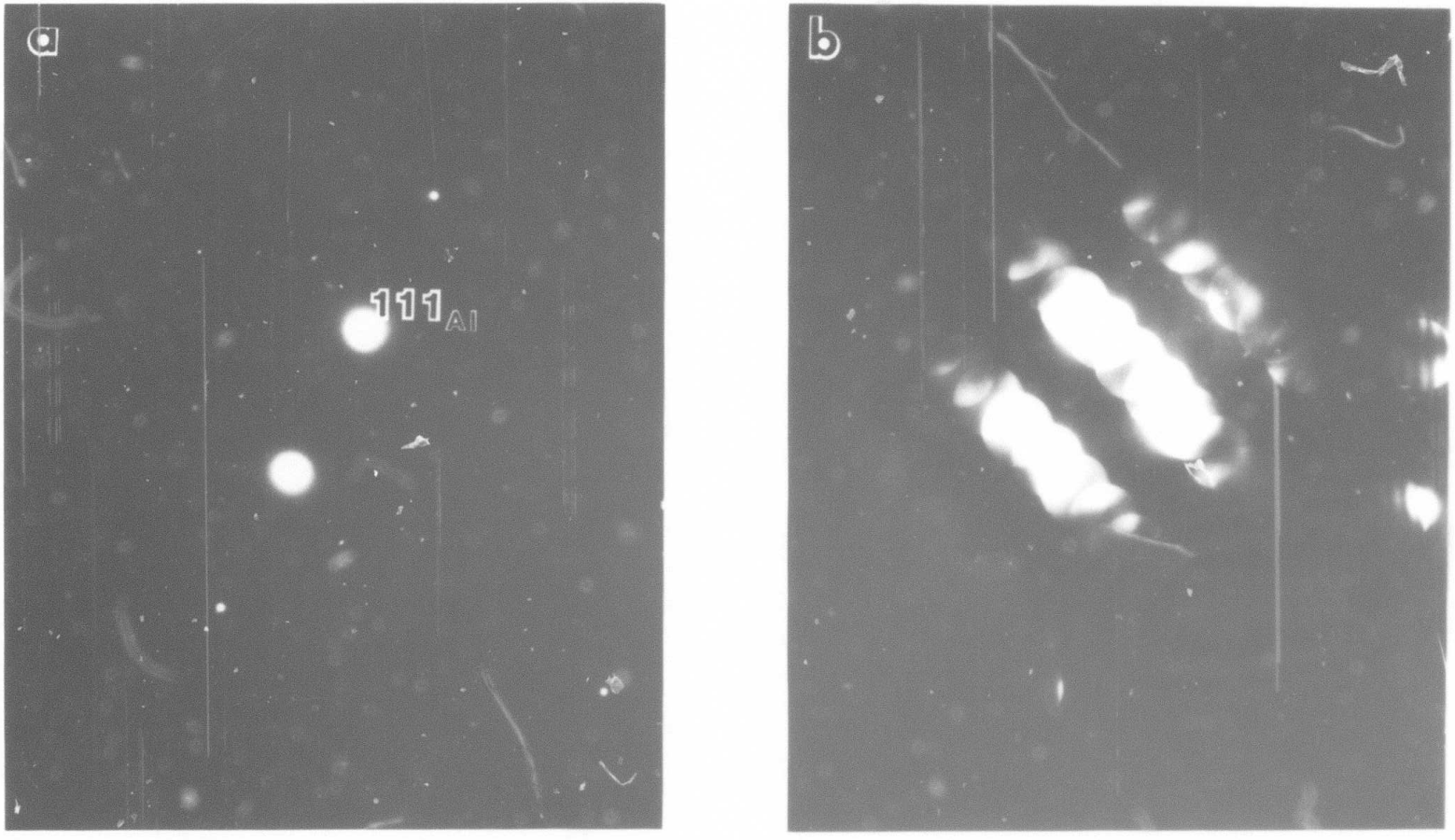

Fig. 4. Diffraction patterns showing the precipitates are $Al_9(Fe,Ni)_2$ phase.
a) SADP, $\overline{B}=[020]_{Al_9(Fe,Ni)_2}$; b) microdiffraction, $\overline{B}=[012]_{Al_9(Fe,Ni)_2}$

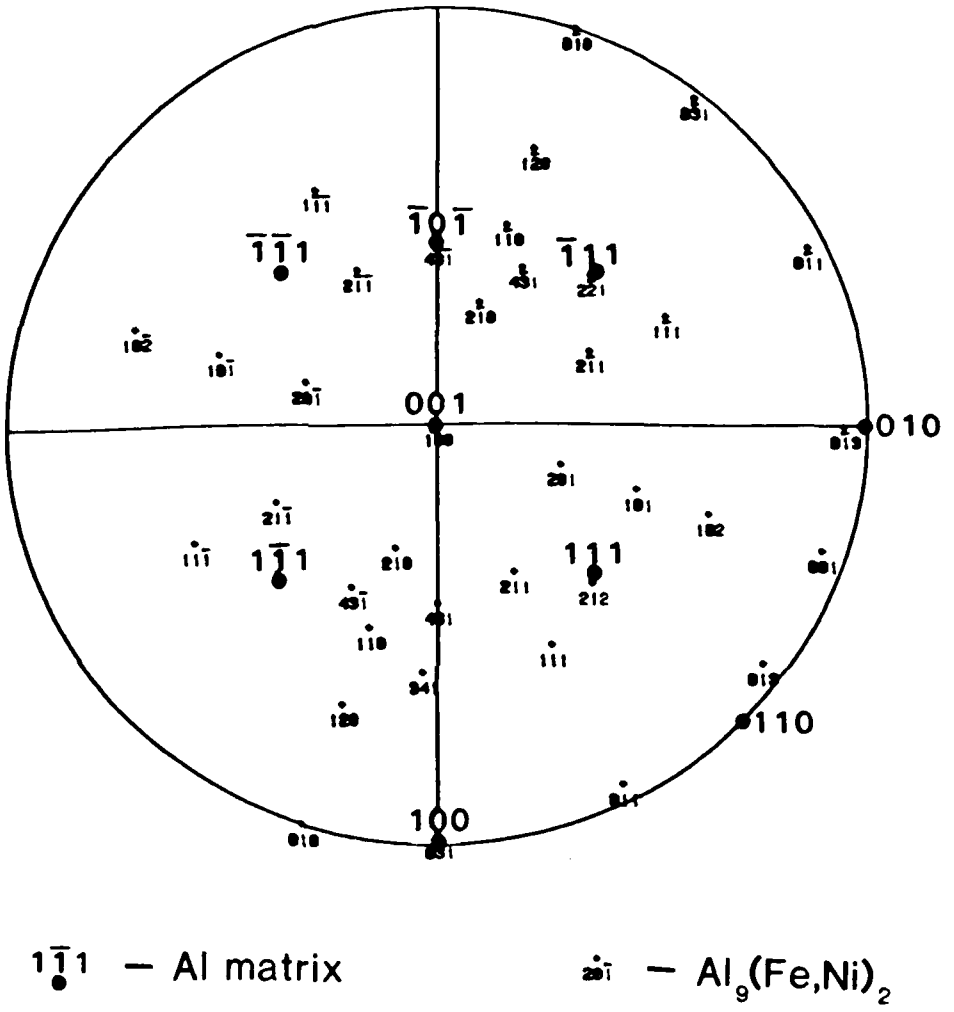

Fig. 5. Superimposed stereographic projections of Al and $Al_9(Fe,Ni)_2$, describing orientation relationship $(100)_{Al_9(Fe,Ni)_2}//(001)_{Al}$ and $(0\bar{3}1)_{Al_9Fe,Ni)_2}//(\bar{1}00)_{Al}$, as well as relationship $(2\bar{2}1)_{Al_9(Fe,Ni)_2}//(\bar{1}11)_{Al}$ and $(43\bar{1})_{Al_9(Fe,Ni)_2}//(101)_{Al}$.

for the Al-Al_9Co_2 eutectic [1,2]; 2) the condition of small coherency mismatch between the precipitate disc plane and the Al matrix, i.e., $d_{020_{Al}} = 0.2025$ nm and $d_{031_{Al_9(Fe,Ni)_2}} = 0.2007$ nm.

To verify the proposed orientation relationship, the diffraction pattern expected for the [110] zone axis of the Al matrix was computed. Twenty-four different variants of the orientation relationship were included (3 of $(100)_{Al_9(Fe,Ni)_2}//\{001\}_{Al}$ type x 8 of $(031)_{Al_9(Fe,Ni)_2}//\{001\}_{Al}$ type)[1]. Fig. 6 shows the computed SADP for the $[110]_{Al}$ axis zone, including possible double diffraction. Comparison with the experimental SADP (Fig. 3a), is as expected. However, there is a slight difference in the interplanar angles between experimental and calculated patterns. The calculated angle between $\bar{g} = (200)_{Al_9(Fe,Ni)_2}$ and $\bar{g} = (01\bar{2})_{Al_9(Fe,Ni)_2}$ (angle between 01 and 03 in Fig. 6) is 94°. The experimentally determined angle between the same $\bar{g}$'s is 92°, which for the same lattice parameters used for calculation Fig. 6, requires β=92.2°. This is smaller than β from

[1]Number of variants was calculated according to the Cahn/Kalonji theory of the symmetry in solid state transformation morphologies [18]. The aluminum matrix belongs to the m3m point group of order 48. $Al_9(Fe,Ni)_2$ monoclinic phase is $P2_1/a$, point group 2/m of order 4. Proposed orientation relationship is

$$(100)_{Al_9(Fe,Ni)_2} \parallel (100)_{Al} \qquad \bar{1} \text{ on } 4/m$$

$$(031)_{Al_9(Fe,Ni)_2} \parallel (010)_{Al} \qquad \bar{1} \text{ on } 4/m$$

The intersection group is $\bar{1}$, triclinic of order 2. There are 24 (48:2) variants.

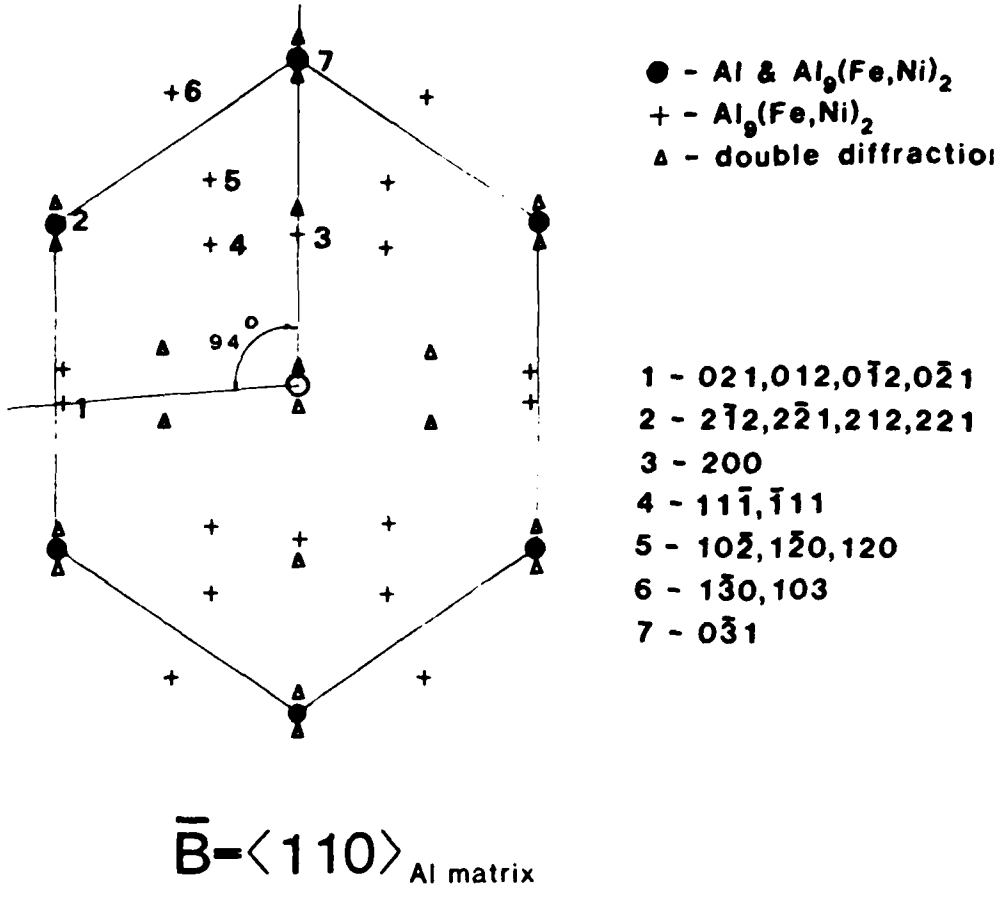

Fig. 6. The superimposed calculated diffraction pattern $\bar{B}=[110]_{Al}$ for 24 variants of matrix/precipitates orientation relationship. The $Al_9(Fe,Ni)_2$ reflections on positions 1 to 7 are listed.

references [5] and [10]. Two possible reasons for the discrepancy should be considered. First, the specific thermodynamic condition of the solid state reaction defines the composition of the precipitates. This composition might be slightly different from the composition of the phase obtained during solidification in [5,10], and the differences in lattice parameters are expected. Secondly, according to the classical scheme of precipitation in other alloys like Aℓ-Cu, the formation of a metastable phase, minimizing strains due to coherency, could precede the formation of stable phase. In our case, the tetragonal phase, which differs from monoclinic only in that $\beta=90°$ instead of 93.4° and b=c for $A\ell_9(Fe,Ni)_2$, could provide better coherency. Subsequent growth of the precipitate releases the distortion elastic strain by gradual transformation of the metastable phase to the stable monoclinic phase. To verify these ideas, much more experimental work is needed, as for example, study of initial stages of precipitation and of the lattice parameter dependence on composition of the precipitated phase.

Finally, we want to point out that, due to a wide range of stoichiometry of ternary $(A\ell_9(Fe,Ni)_2$ phase and to the strong orientation relationship with the Aℓ matrix, the optimum coherency with the matrix might be obtained by changing the nominal composition of the alloy. Hence, maximum thermal stability of precipitates could be obtained.

ACKNOWLEDGEMENTS

Appreciation is extended to Drs. W. J. Boettinger and M. J. Kaufman for valuable discussions and comments on the manuscript. Thanks due to Drs. G. J. Hildeman and R. Rioja from Alcoa Tech. Center for pointing out the interesting microstructure of Aℓ-Fe-Ni alloys. The author acknowledges the support of DARPA.

REFERENCES

1. S. Marich, J. Aust. Inst. Metals, 1972, Vol. 17, p. 18.

2. C. Mc. L. Adam, S. Marich, J. Aust. Inst. Metals, 1972, Vol. 17, p. 142.

3. T. M. Sanders, Jr., J. W. Johnson, and E. E. Underwood, in Proc. of the Second International Conference of Rapid Solidification, Reston, Virginia, March 1980, Claitor's Publishing, Baton Rouge, La., pp. 141-151.

4. T. M. Sanders, Jr., M. G. Paris, and J. W. Mullins, in Rapidly Solidified Amorphous and Crystalline Alloys, Eds., B. M. Kear, B. C. Giessen, and M. Cohen, (1982), pp. 369-374.

5. F. M. Froes and J. R. Pickens, J. of Metals, January 1984, p. 14.

6. C. J. Simensen and R. Vellasamy, Z. Metallkde, 1977, Vol. 68, p. 428.

7. W. H. Phillips, J. Inst. of Metals, 1942, Vol. 68, p. 27.

8. G. V. Raynor and P. C. Pfeil, J. Inst. Metals, 1947, Vol. 73, pp. 397-419.

9. L. F. Mondolflo, Aluminum Alloys Structure and Properties, 1979, Butterworths, London, p. 532.

10. V. G. Rivlin and G. V. Raynor, Inter. Metals Reviews, 1980, No. 3, pp. 37-93.

11. M. Khaidar, C. M. Allibert, and J. Driole, Z. Metallkde, 1982, Vol. 73, p. 433.

12. G. J. Hildeman, G. J. Lege, and A. K. Vasudevan, "Fundamentals of Compaction Processes for Rapidly Quenched Prealloyed Metal Powders," 1982, Final Report APWAL Contract F33615-79-0-5037.

13. G. J. Hildeman, D. J. Lege, and A. K. Vasudevan, in High-Strength Powder Metallurgy Aluminum Alloys, The Metallurgical Society of AIME, 1982, p. 249.

14. W. J. Boettinger and L. Bendersky, to be published.

15. J. C. Baker and J. W. Cahn, Solidification, ASM, Metals Park, Ohio, 1971, p. 23.

16. S. R. Coriell and R. F. Sekerka, Rapid Solidification Processing, Principles and Technologies, II, R. Mehrabian, B. M. Kear, and M. Cohen, Eds., Claitor's, Baton Rouge, La., 1980, pp. 35-49.

17. W. J. Boettinger, S. R. Coriell, and R. F. Sekerka, Third Conference of Rapid Solidification Processing, held at NBS in December 1982, R. Mehrabian, Chairman.

18. J. W. Cahn and G. Kalonji, Inter. Conf. on Solid/Solid Phase Transformations, Met. Soc. of AIME, 1981, p. 3.

RAPIDLY SOLIDIFIED Aℓ-Cr ALLOYS: STRUCTURE AND DECOMPOSITION BEHAVIOR

L. BENDERSKY

Center for Materials Research
The Johns Hopkins University
Baltimore, Maryland 21218

R. J. SCHAEFER, F. S. BIANCANIELLO

Metallurgy Division
Center for Materials Science
National Bureau of Standards
Washington, D. C. 20234

D. SHECHTMAN

Department of Materials Engineering
Technion
Haifa, Israel
and
Center for Materials Research
The Johns Hopkins University
Baltimore, Maryland 21218

To be published in the Journal of Materials Science.

I. INTRODUCTION

Transition metals are commonly used as alloying elements to aluminum. Although they do not produce age hardening, they are added for various purposes, such as mechanical property improvement, recrystallization inhibition, stress corrosion prevention, etc. Due to the unfavorable electrochemical factor and the tendency of the components to form intermetallic phases, the range of solid solubility is extremely limited. It can, however, be significantly extended by rapid solidification [1-3]. The substantial increase in solid solubility offers the prospect of developing new alloy compositions with improved thermal stability. Several such additives like Cr, Mn and Zr offer resistance to solute clustering during (or following) quenching [4,5].

Rapidly solidified Al-Cr alloys exhibit a pronounced tendency to form metastable supersaturated solid solutions. This system has been investigated by various authors [5-15] who used different techniques of rapid quenching from the melt. Most previous studies [10-12, 14-15] were limited to compositions of up to 3 wt% Cr, and some of them lack microstructural studies. Detailed electron microscopy investigation was performed by H. Warlimont and co-workers [8,9] and H. Jones and co-workers [2,5,6]. Their studies were performed on compositions of up to 13 wt% Cr, and included study of the decomposition behavior. These publications are the main references for us.

In the present study we examined the microstructure of melt-spun ribbons which contain up to 15 wt% Cr. Thermal

stability and decompositional behavior were studied as a function of the Cr content and the temperature of isochronal heat treatment.

2. Experimental

Alloy buttons with Cr concentration of 1, 2, 5, and 15 wt% Cr were prepared by arc melting, using 99.999% Aℓ and 99.95% Cr. For melt-spinning, small pieces cut from these buttons were induction heated in zirconia-coated quartz tubes. Immediately upon melting, the metal was squirted onto a copper melt-spinning wheel rotated at 6500 rpm. The process was carried out under helium at atmospheric pressure. The ribbons were typically 2mm wide and 20μm thick. For annealing, the ribbons were sealed in borosilicate glass ampoules with a helium pressure of 1/2 atmosphere.

Lattice parameters were determined by measurements on an x-ray diffractometer, using filtered Cu K_α radiation. A Nelson-Reiley procedure was used to obtain the lattice parameter from the measurements of the diffraction peaks. Simultaneous measurement of diffraction peaks from powdered high purity silicon were used as a normalization standard.

Three phases of apparently very similar crystal structure have been reported in Aℓ rich Aℓ-Cr alloys [16]: $Aℓ_7Cr$ or θ (21.6 wt% Cr), $Aℓ_{11}Cr_2$ or η (25.96 wt% Cr) and $Aℓ_4Cr$ or ε (32.52 wt% Cr) are reported [9] to be very similar and no information on differences between them have been reported. We therefore prepared samples having the stoichiometric

compositions of these compounds as x-ray diffraction references. These samples were first melt spun to reduce microsegregation, crushed and sieved to -325 mesh, and annealed at 600°C for 16 hours. X-ray diffraction patterns from these powders, using Cu K_α radiation, were then compared.

Microstructural studies were performed on a Philips 400 scanning transmission electron microscope. Chemical microanalysis was performed in the scanning transmission mode using a 5 nm probe. Quantification of the x-ray information was accomplished by using the Cliff-Lorimer method [17,18], when the condition of the thin film approximation was maintained. X-ray intensity relates to composition by the expression $C_A/C_B=k_{AB}\ I_A/I_B$, where I_A and I_B are the measured characteristic x-ray intensities, and C_A and C_B are the weight fractions of two elements A and B (in our case Aℓ and Cr). The coefficient $k_{Cr/A\ell}$ (constant in the thin film approximation) was found experimentally using the known phase $A\ell_7Cr$ as a standard: $k_{A\ell/Cr}=0.91 \pm 0.1$.

The ribbons were thinned for STEM study by jet electropolishing in a standard solution.

3. Results

3.1 As-spun ribbons (TEM analysis)

The 1 and 2 wt% Cr alloys are one-phase supersaturated solid solution of Cr in Aℓ (maximum equilibrium solubility is 0.77 wt% Cr [18]). No second phase can be observed. A dislocation substructure is present and is probably associated with slight cellular microsegregation (see Fig. 1).

The 5 wt% Cr alloy has a transition microstructure between low and high concentration of Cr. In some regions the microstructure consists of one-phase grains of supersaturated (5 wt% Cr) α-Aℓ, with slight evidence of cellular structure and dislocation substructure (like the 1 and 2 wt% Cr alloys). In other regions the microstructure is characterized by multiphase spherulites, embedded in α-Aℓ matrix. Their volume fraction increases with increase of chromium concentration to reach homogeneous high density in the 15 wt% Cr alloy (see Fig. 2). The formation of spherulites was reported for the Aℓ-Cr system by authors [9] and for several other systems by [19].

The spherulites are generally composed of a core A (see Fig. 3a), surrounded by small petal-like crystals B measuring ∿50 nm in size. The contrast of the petals is sometimes enhanced by Moire fringes. The core has a two-phase structure, composed of very fine particles of size smaller than 5 nm. In some cases the spherulites are without petals on the periphery, as was found in [9]. Chemical microanalysis shows that the average composition of the core is 22 ± 2 wt% Cr. The composition of the matrix surrounding the spherulites is ∿5 wt% Cr. A typical concentration profile of the microstructure is shown in Fig. 4, where gradual transition from 22 to 5 wt% Cr reflects a decrease in the density of petals embedded in the α-Aℓ matrix. Dark field micrographs obtained with an Aℓ reflection (see Fig. 3b) confirms that the surrounding matrix is α-Aℓ. A series of convergent beam diffraction patterns

taken from different spherulites in the same matrix show that the spherulites are randomly oriented. These diffraction patterns are a combination of two or more single patterns of intermetallics with orientational coherence between them. No aluminum reflections were found here. This contradicts some results obtained by authors [9] who concluded that spherulites are composed of randomly oriented precipitates within the Aℓ matrix.

Analysis of convergent beam diffraction patterns from the petals shows that they have the structure of the θ phase ($Aℓ_7Cr$) (see Fig. 5), which is monoclinic with a = 2.531 nm; b = 0.754 nm; c = 1.0949 nm; β = 128°71' [20]. Dark field micrographs (Fig. 6) obtained with an intermetallic reflection show the possibility that the petals and at least one group of fine precipitates in core have the same structure.

3.2 Heat treated ribbons (TEM analysis)

The decomposition behavior of the alloys was studied in the range of temperatures 250°C to 550°C for composition of 1, 2, and 5 wt% Cr. For most cases the annealing time was 6 hours, however for some up to 100 hours. Generally, super-saturated Aluminum decomposes at the grain boundaries and within grains to form needle- or plate-like precipitates of the equilibrium phase $Aℓ_7Cr$, with no indication of any transition phase, in agreement with [5, 6, 15].

Analysis of samples annealed for 6 hours shows that grain boundary precipitation (GBP) starts at a lower temperature

than matrix precipitation (MP). The difference is roughly 50°C. The temperature at which decomposition starts (where the second phase is first observed) depends strongly on the degree of supersaturation. Fig. 7 shows the summarized results, where the curves represent the beginning of the GBP and MP decomposition. Annealing up to 100 hours at temperatures of GBP start results in the appearance of only GB precipitates, without any matrix precipitation (see Fig. 8). At temperatures above the MP start curve, fast growth of matrix precipitates occurs, until the supersaturated matrix is completely relaxed (see Fig. 9). Selected area electron diffraction indicates that both grain boundary and matrix precipitates are A_7Cr (θ phase) (Fig. 10). It was found the longest axis of the precipitates is parallel to the <011>Aℓ direction.

The microstructure after annealing at temperatures below the curve of GBP start (Fig. 7) is characterized by finely dispersed strain contrast (see Fig. 11). No distortion of diffraction spots or super-lattice reflections were found. Annealing at higher temperatures for longer time does not change the character of diffraction, but the contrast appears to be more intensive (Fig. 12) and the centers of strain contrast are less dense. In certain cases it is possible to resolve it as loops (Fig. 13). These loops or clusters have very high thermal stability and exist up to 500°C (see Fig. 14).

3.3 X-ray Studies

The measured lattice parameters of the as-spun 1, 2, and 5 wt% Cr ribbons are in agreement with those previously reported [5, 12] for rapidly solidified alloys (Fig. 15). No indication of phases other than Aℓ is seen in the x-ray diffraction patterns of these alloys. Upon annealing for 6 hours, no significant change of lattice parameter is seen at temperatures of 400°C or less. At 450°C the lattice parameter of the 5 wt% Cr alloy has started to shift, and at 500°C the supersaturation of the 5% and 2% alloys has mostly disappeared (Fig. 15).

X-ray diffraction peaks from intermetallic phases are first seen after 6 hours at temperatures as low as 400°C (Fig. 16) and become progressively stronger at higher temperatures. Analysis of alloys having stoichiometric compositions shows that only the $Aℓ_7Cr$ sample had a peak at $2\theta=21.7°$, only the $Aℓ_4Cr$ sample had peaks at $2\theta=17°$ and 26.6°, and the $Aℓ_{11}Cr_2$ sample showed none of these peaks. In addition, there was a substantial difference in the detailed distribution of intense peaks in the region between 2θ = 36-46°, with the pattern computed from structural data reported for $Aℓ_7Cr$ [20] as shown in Fig. 16. It should be noted that the diffraction patterns of these samples were significantly different before and after annealing at 600°C, as would be expected from the phase diagram.

On the basis of the diffraction patterns of the reference samples, the precipitates in the annealed ribbons are identified

as shown in Fig. 17. In the earlier stages of precipitation, however, the phase identification can only be tentative.

The diffraction pattern of the as-spun 15 wt% Cr alloy shows strong intermetallic peaks not seen in the reference samples. After annealing for 6 hours at 350°C or higher, intermetallic peaks clearly corresponding to $A\ell_7$ Cr are observed. It cannot be determined from the x-ray diffractometer patterns alone whether the peaks in the as-spun 15 wt% Cr ribbon are the result of a distortion of one or more of the phases mentioned above, or are due to yet another, metastable, phase. Other authors [9] have reported mixtures of the different phases in rapidly solidified Aℓ-Cr alloys, with increasingly rapid solidification tending to suppress the peritectic formation of the θ phase.

4. Discussion

Highly extended solid solubility can be achieved for melt-spun ribbons of Aℓ-Cr. In our experiments the extension is up to 5 wt% Cr, and we believe that it is close to the maximum obtainable by the technique of melt quenching. The maximum was established to be 7 wt% Cr for two-piston [5] and splat [9] quenching for a thickness of ∿50 μm. Higher values, up to 10 wt% Cr, were attainable for very thin sections, e.g., of gun splats [8, 9, 21]. These differences in solid solubility maximum reflect the sensitivity to the changes in the cooling rate in the range 10^6 K/s to 10^8 K/s, and to the degree of supercooling [7].

Aluminum containing small concentrations of Cr is expected to solidify without microsegregation at relatively low velocities on the basis of the absolute stability effect of morphological stability theory [22]. Because the solute partition coefficient in this system is relatively close to unity (although not known with precision), the absolute stability effect is predicted to occur at relatively low velocities (or high concentrations) compared to a system such as Aℓ-Fe [19], where the solute partition coefficient is extremely small. This effect accounts for the absence or rarity of cellular substructures in the alloys containing 1, 2, or 5 wt% Cr.

At higher concentration (>5 wt% Cr) the competitive solidification of intermetallic phases begins. They appear within the liquid and grow of spherulites to ∿1 μm diameter before being engulfed by the solidifying supersaturated aluminum front. The spherulite volume density increases with increasing chromium concentration. For the 15 wt% Cr alloy the solidification of spherulites is the dominant mode. The appearance of spherulites influences the mechanical properties. For example, Yakunin et al. [23] reported decreasing tensile strength for alloys with composition higher than 8 wt% Cr. Solidification as separated spherulites is an unusual pattern in rapid solidification, although common in concentrated aluminum-transition metal alloys, e.g., in Aℓ-Fe (>11 wt% Fe) and Aℓ-Mn (>15 wt% Mn) [19, 24]. The increase of spherulite volume density points out that the

nucleation rate for the intermetallic phase starts to be dominant compared to the nucleation rate for α-Aℓ as the concentration of the alloy increases. The steep increase of the intermetallic liquidus with concentration, compared to the slow change for the α-Aℓ liquidus, provides different rates of change in supercooling with concentration. The supercooling as a function of chromium content changes very little for α-Aℓ, while it strongly increases for the intermetallic. Accordingly, the relative nucleation rate depends on the concentration.

Equilibrium freezing concepts would predict that in the 5 wt% Cr alloy the η phase would form first from the liquid and the ϑ phase would then form by a peritectic reaction, whereas in the 15 wt% Cr alloy, primary ε phase would form, followed by peritectic η and θ. Under rapid solidification conditions, however, the equilibrium phases may be suppressed. The core of the spherulites formed in the 15 wt% Cr alloy, which has a composition midway between that of the θ and η phases, could thus have initially solidified from the melt as any of the intermetallic phases and subsequently decomposed in the solid state during cooling of the ribbon into a mixture of ϑ and η.

It should be noted that the equilibrium boundaries of the ϑ, η, and ε phases are not well established, and the θ and η phases are reported to be structurally identical [25]. The exact identification of the many very fine crystallites which

appear in the rapidly solidified materials is therefore difficult, and even the prediction of the relative stability of the different phases is questionable.

REFERENCES

1. H. Jones, Aluminum, 54, 274 (1978).

2. S. P. Midson, H. Jones, in Proc. 4th Int. Conf. on Rapid Quchehed Metals (Sendai, 1981), p.

3. G. Falkenhagen, W. Hofmann, Z. Metallk, 43, 69 (1952).

4. H. James in "Vacancies 26," R. E. Smallman and J. E. Morris, Eds., p. 175.

5. S. P. Midson, R. A. Buckley and H. Jones, in Proc. 4th Conf. on Rapidly Quenched Metals (Sendai, 1981).

6. H. Jones in Rapid Solidification Processing, Principles and Technology II, ed. R. Mehrabian, B. Kear, and M. Cohen, Claitor's , Baton Rouge (1980), p. 306.

7. R. Ichikawa, T. Ohashi, T. Ikeda, Trans. JIM, Vol. 12, 280, 1921.

8. H. Warlimont, W. Zingg, P. Furrer, Mat. Sci. Eng. 23, 101, 1976.

9. P. Furrer, H. Warlimont, Mat. Sci. Eng., 28, 127 (1977).

10. N. I. Varich, R. B. Zyukevich, Russian Metallurgy 4, 58 (1920).

11. N. I. Varich, R. B. Zyukevich, Izv. Acad. Nauk, Met., 4, 82 (1970).

12. A. F. Polesya, A. I. Stepina, Fiz. Met. Metallov., 27 (5), 885 (1969).

13. R. D. Vengrenovich, V. I. Psarev, Fiz. Met. Metallov., 29 (3), 540 (1970),

14. V. I. Dobatkin et al., Izv. Acad. Nauk, Metalli, 2, 199 (1920).

15. K. Nagahama, I. Mike, Trans. JIM, 15, 185 (1924).

16. A. J. Bradley and S. S. Lu, J. Inst. Metals 60, 319 (1937).

17. G. Cliff, G. W. Lorimer, J. Microsc., 62, 246 (1975).

18. N. J. Zaluzec in Introduction to Analytical Electron Microscopy, ed. J. J. Hren, J. I. Goldstein, D. C. Joy, p. 121 (1979).

19. D. Shechtman and E. Horowitz, "Metastable Phases of Rapidly Solidified Aℓ-Rich Aℓ-Fe Alloys," Quarterly Report DARPA Order No. MDA-903-83-K-0400, January 1984.

20. M. J. Cooper, Acta Cryst., 13, 257 (1960).

21. L. M. Burov, A. A. Yakunin, Russ. J. Phys. Chem., 42, 540 (1968).

22. S. R. Coriell, R. F. Sekerka, J. Crystal Growth, 61, 499 (1983).

23. A. A. Yakunin, L. F. Silka, A. B. Lisenko, Fiz. Met. Metalloved., 56 (5), 945 (1983).

24. D. Shechtman, private communication.

25. R. P. Elliott, Constitution of Binary Alloys, First Supplement, McGraw-Hill, New York (1965) p. 33.

Figure Captions

Figure 1. As-spun ribbon of Al-2 wt% Cr alloy. A dislocation substructure is probably associated with slight microsegregation.

Figure 2. As-spun ribbon of Al-15 wt% Cr alloy. Spherulites embedded in Al matrix.

Figure 3. As-spun ribbon of Al-15 wt% Cr.
a) Bright field image of spherulites. The spherulites are composed of a core A, surrounded by petal-like crystals B (marked by arrows).
b) Dark field using an Al-matrix reflection. Surrounding matrix is α-aluminium.

Figure 4. Composition profile across a spherulite.

Figure 5. Microdiffraction from the "petal." [110] zone axis of Al_7Cr. Arrows show directions (00ℓ) and (hhh) of reflection rows.

Figure 6. Dark field using an intermetallic reflection. Fine precipitates in spherulite core and some petals (marked by arrows) reflect at the same time.

Figure 7. Annealing temperature-composition diagram, where curves represent the beginning of precipitation on grain boundaries (GBP) and inside the grains (MP) for 6 hour anneals.

Figure 8. The Al-2 wt% Cr following 100 hours at 400°C containing Al_7Cr particles mostly along grain boundaries.

Figure 9. The Al-5 wt% Cr following 6 hours at 550°C containing Al_7Cr particles within the grains.

Figure 10. Diffraction pattern typical for both grain boundary and matrix precipitates. [112] axis zone of Al_7Cr.

Figure 11. The Al-5 wt% Cr following 100 hours at 300°C. Dark field using (111) reflection of Al. Finge strain contrast. Diffraction pattern is entirely of aluminium.

Figure 12. The Al-1 wt% Cr following 6 hours at 500°C. Dark field using (111) reflection of Al at weak beam condition. Stain contrast is enhanced compared to Figure 13. Diffraction pattern is entirely of aluminium.

Figure 13. The Al-1 wt% Cr following 6 hours at 450°C. Dark field using (020) reflection of Al at weak beam condition of dislocation loops.

Figure 14. The Al-2 wt% Cr following 6 hours at 500°C. Bright field micrograph shows coexistence of Al_7Cr precipitates and objects of strain contrast.

Figure 15. Latice parameter of Al-Cr alloys, compared to data previously reported in (a) reference (3) and (b) reference (12).

Figure 16. Diffraction patterns of CuK_{α} radiation from samples having the stoichiometric compositons of the Al-Cr intermetallic compounds. Samples were melt spun, crushed, and annealed at 600°C for 16 hours.

Figure 17. Phases observed by x-ray diffraction in melt-spun and annealed Al-Cr ribbons.

Figure 1. As-spun ribbon of Al-2 wt% Cr alloy. A dislocation substructure is probably associated with slight microsegregation.

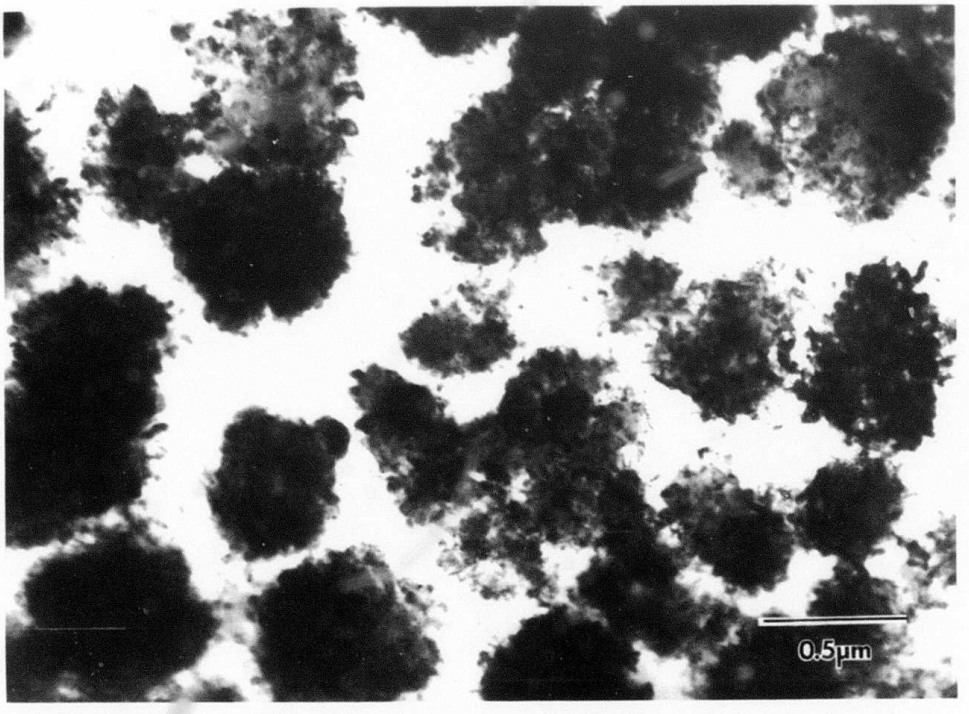

Figure 2. As-spun ribbon of Al-15 wt% Cr alloy. Spherulites embedded in Al matrix.

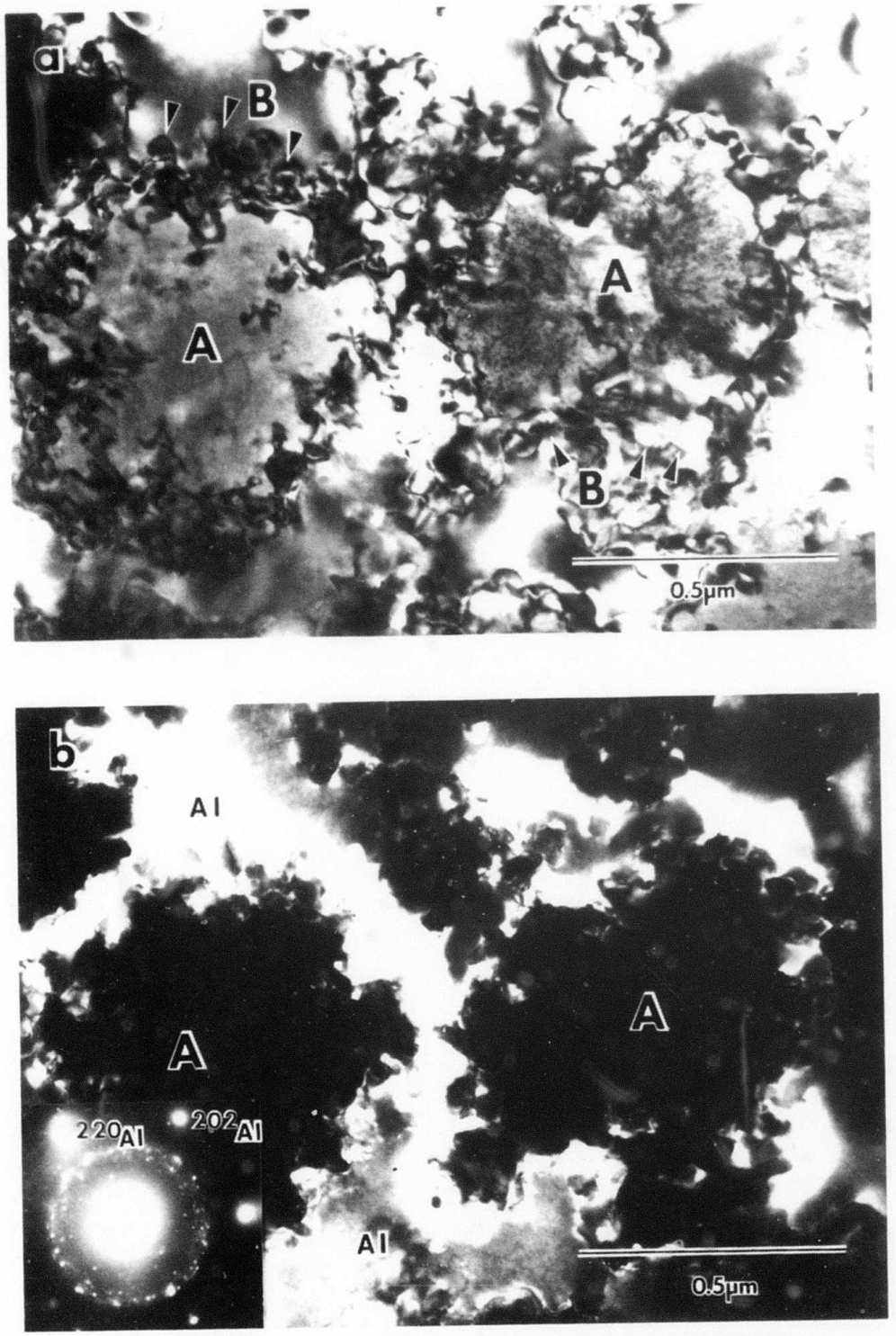

Figure 3. As-spun ribbon of Al-15 wt% Cr.
a) Bright field image of spherulites. The spherulites are composed of a core A, surrounded by petal-like crystals B (marked by arrows).
b) Dark field using an Al-matrix reflection. Surrounding matrix is α-aluminium.

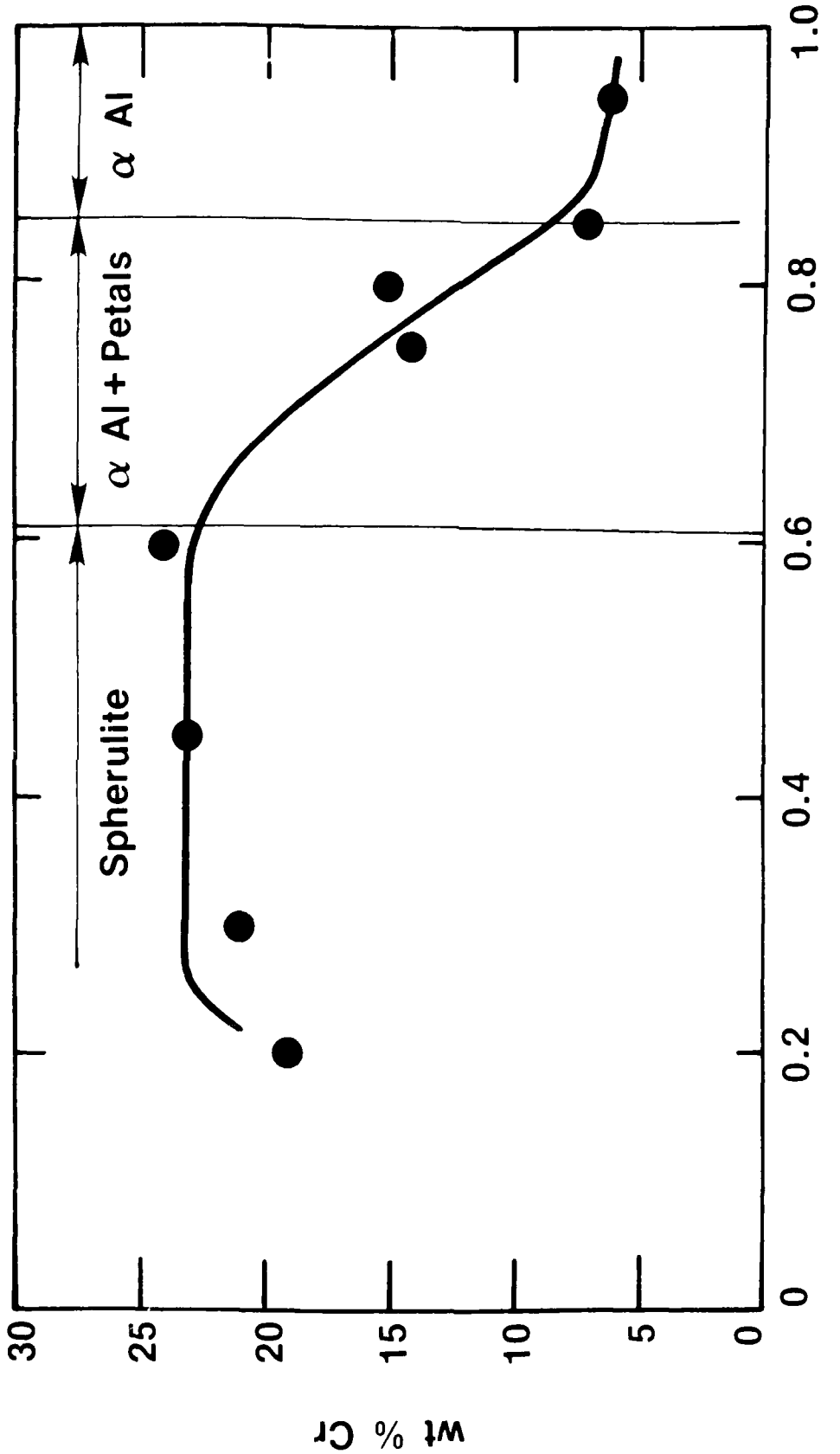

Figure 4. Composition profile across a spherulite.

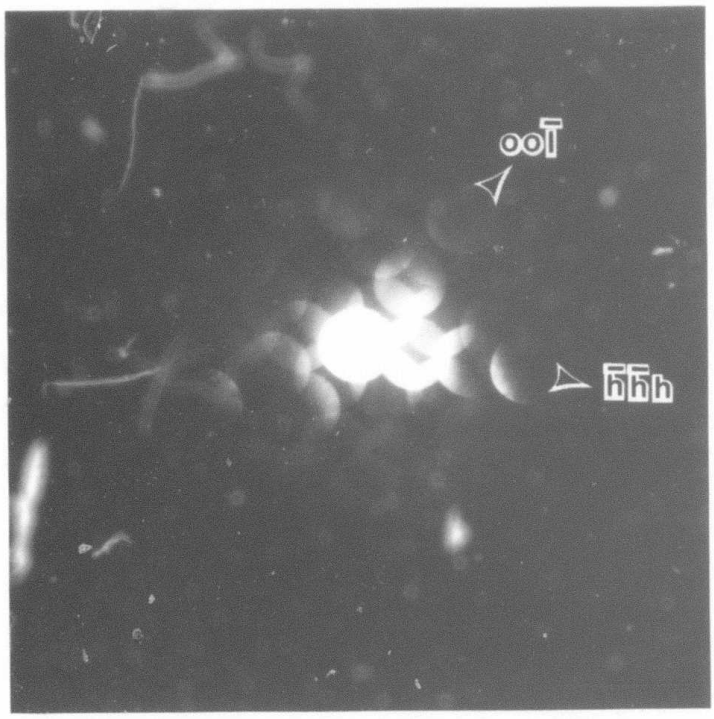

Figure 5. Microdiffraction from the "petal." [110] zone axis of Al_7Cr. Arrows show directions (00ℓ) and (hhh) of reflection rows.

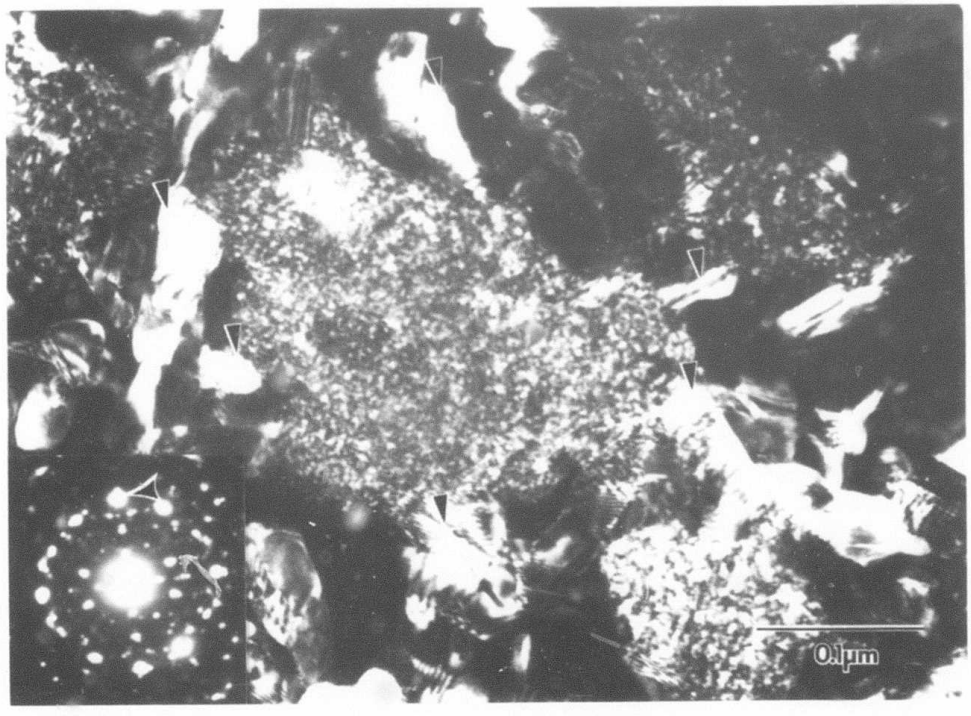

Figure 6. Dark field using an intermetallic reflection. Fine precipitates in spherulite core and some petals (marked by arrows) reflect at the same time.

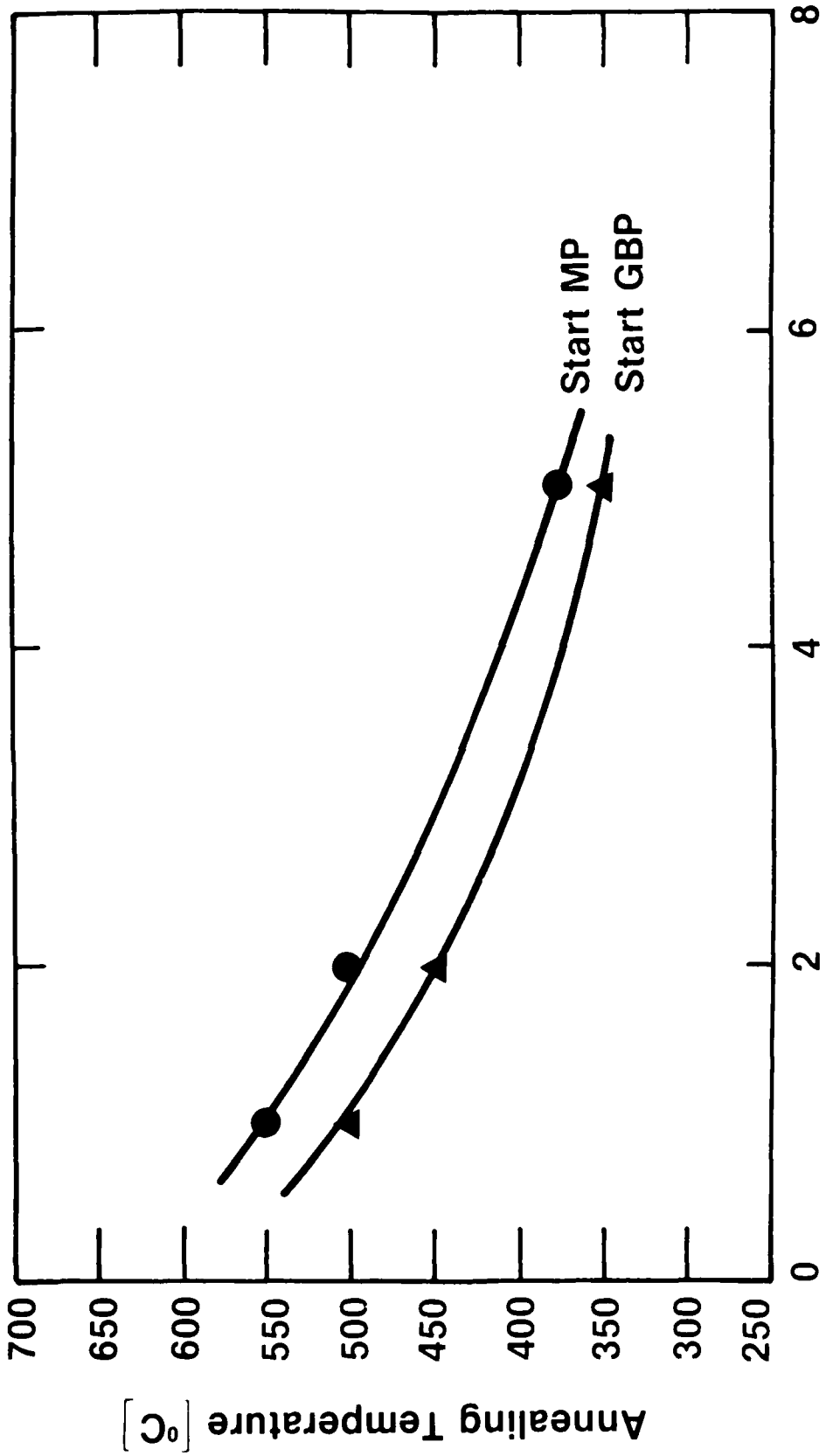

Figure 7. Annealing temperature-composition diagram, where curves represent the beginning of precipitation on grain boundaries (GBP) and inside the grains (MP) for 6 hour anneals.

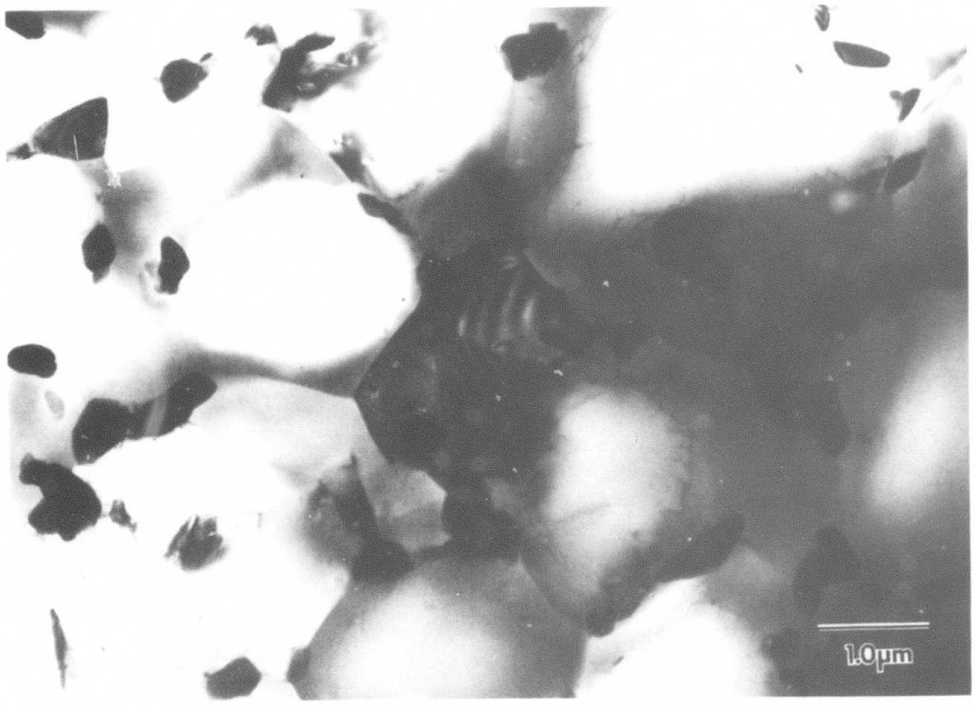

Figure 8. The Al-2 wt% Cr following 100 hours at 400°C containing Al_7Cr particles mostly along grain boundaries.

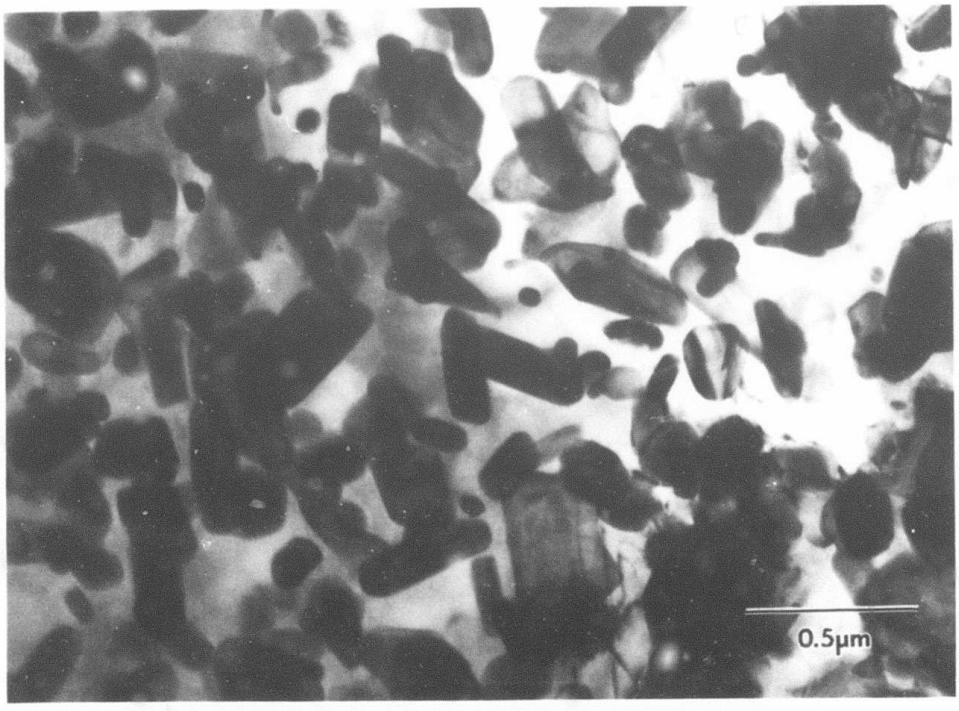

Figure 9. The Al-5 wt% Cr following 6 hours at 550°C containing Al_7Cr particles within the grains.

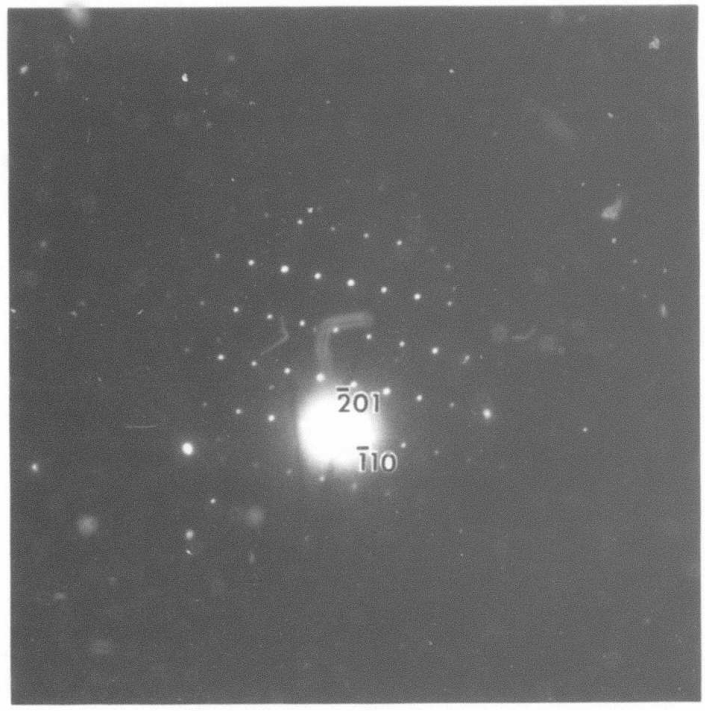

Figure 10. Diffraction pattern typical for both grain boundary and matrix precipitates. [112] axis zone of Al_7Cr.

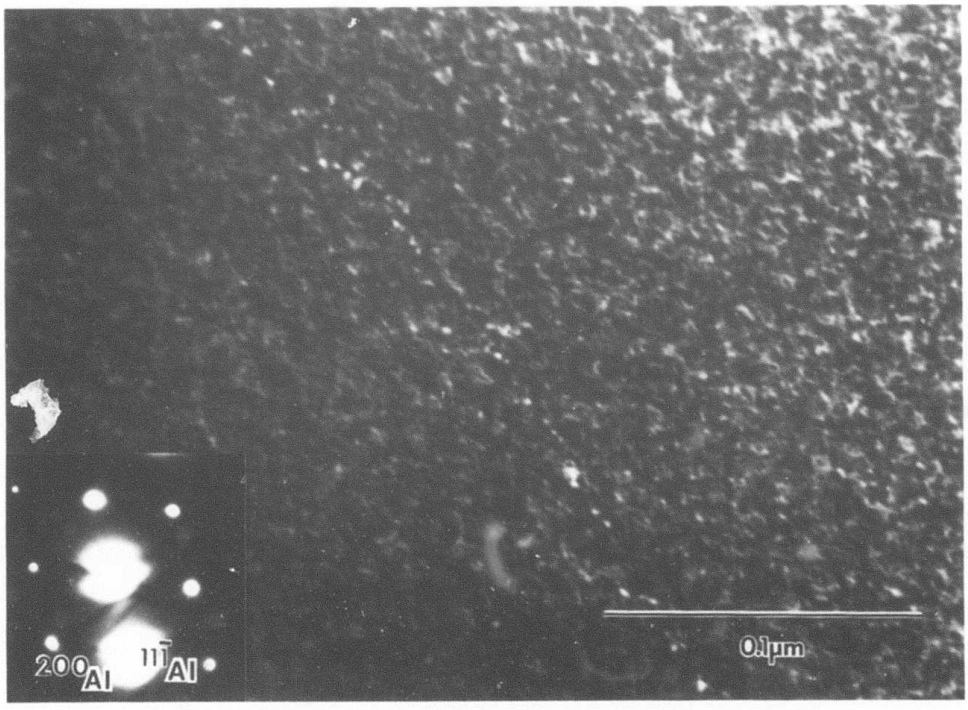

Figure 11. The Al-5 wt% Cr following 100 hours at 300°C. Dark field using (111) reflection of Al. Finge strain contrast. Diffraction pattern is entirely of aluminium.

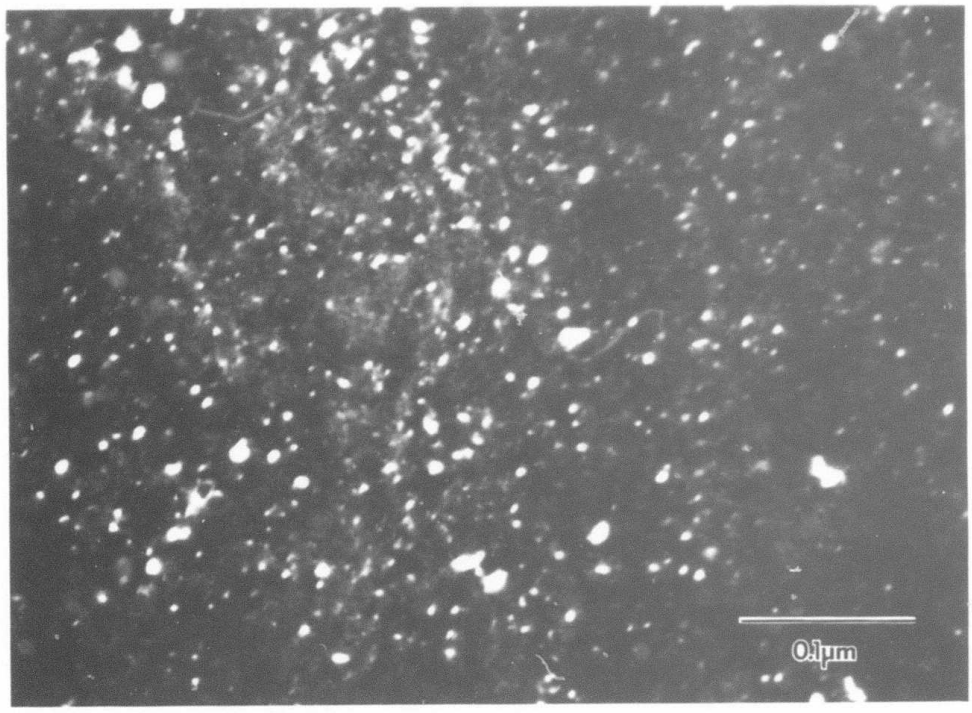

Figure 12. The Al-1 wt% Cr following 6 hours at 500°C. Dark field using (111) reflection of Al at weak beam condition. Stain contrast is enhanced compared to Figure 13. Diffraction pattern is entirely of aluminium.

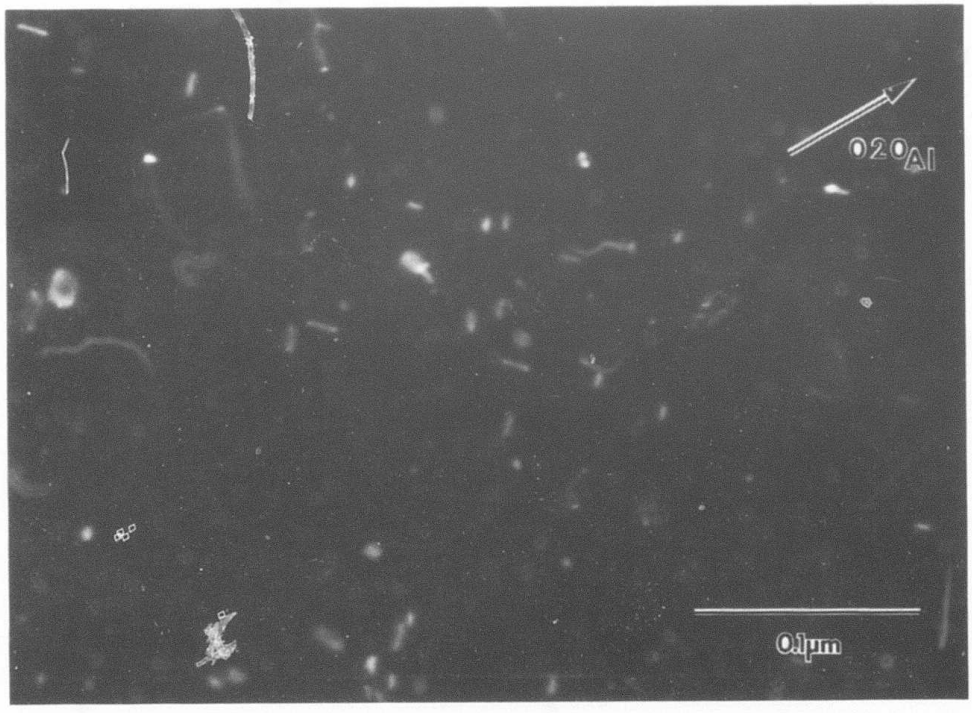

Figure 13. The Al-1 wt% Cr following 6 hours at 450°C. Dark field using (020) reflection of Al at weak beam condition of dislocation loops.

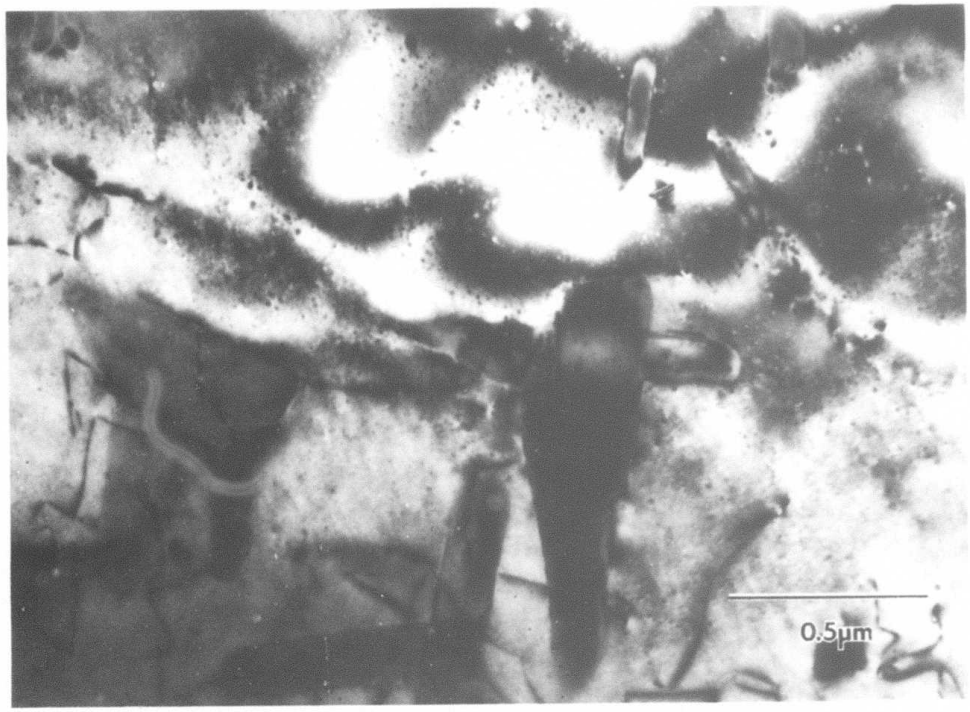

Figure 14. The Al-2 wt% Cr following 6 hours at 500°C. Bright field micrograph shows coexistence of Al_7Cr precipitates and objects of strain contrast.

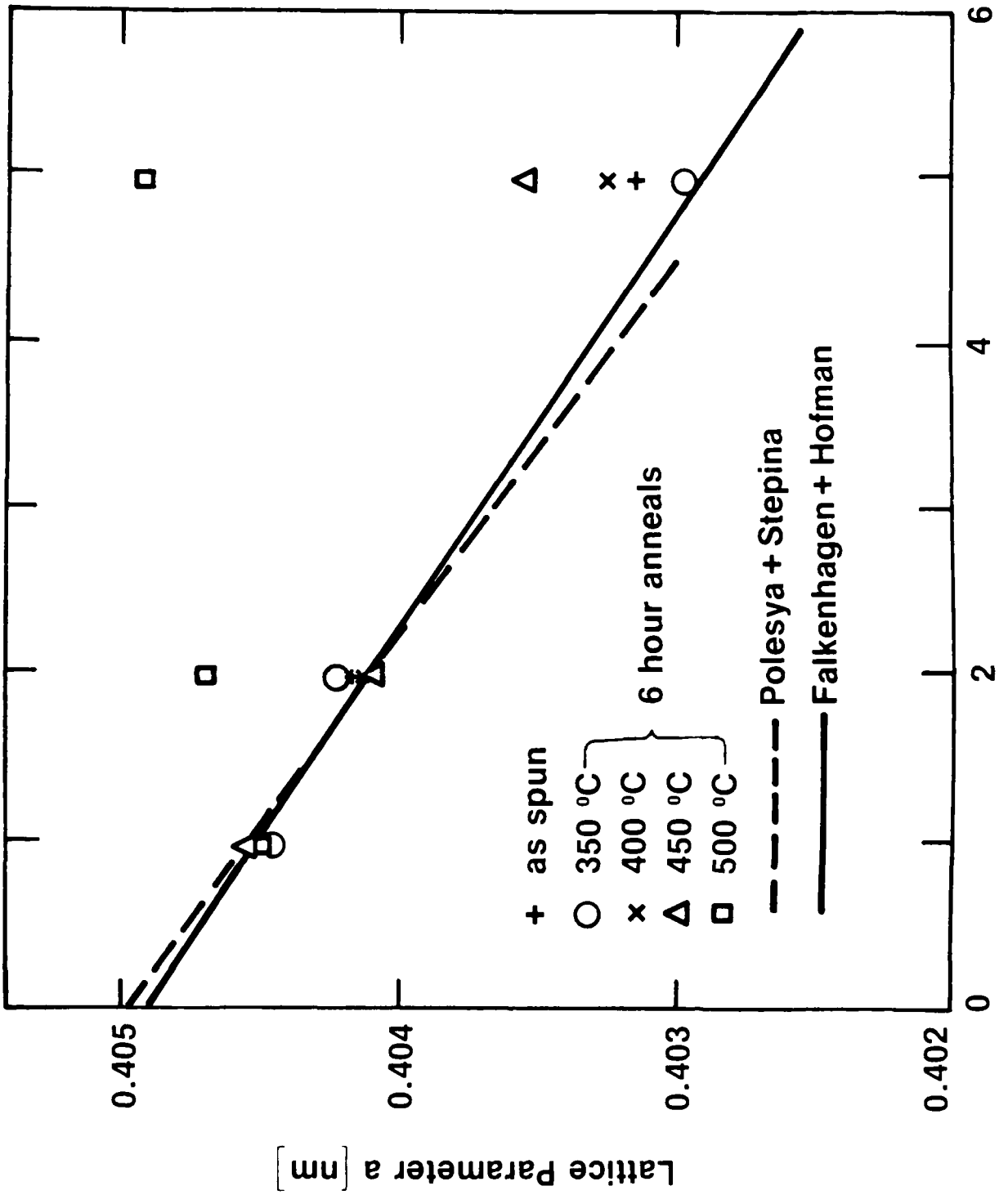

Figure 15. Lattice parameter of Al-Cr alloys, compared to data previously reported in (a) reference (3) and (b) reference (12).

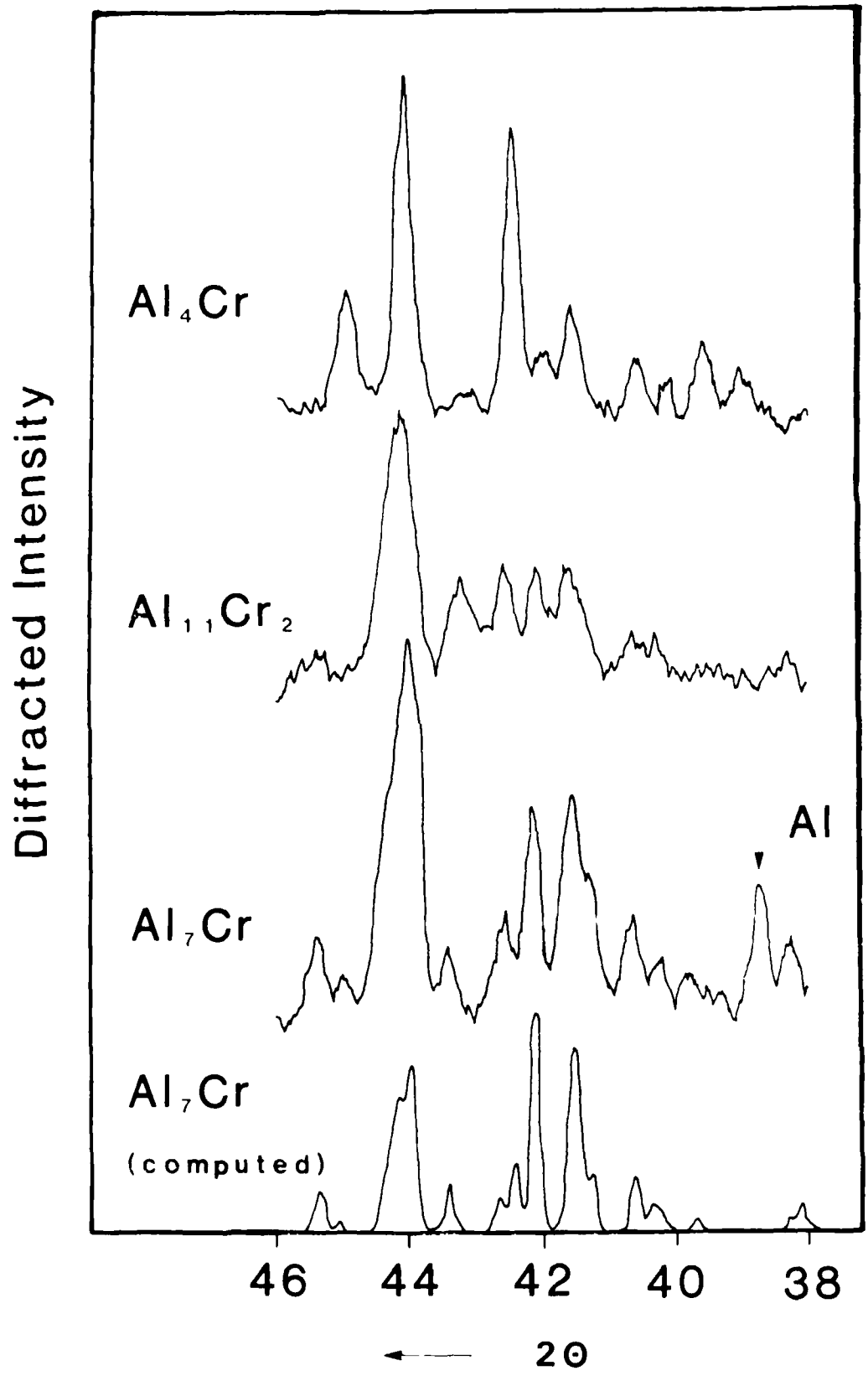

Figure 16. Diffraction patterns of CuK_α radiation from samples having the stoichiometric compositons of the Al-Cr intermetallic compounds. Samples were melt spun, crushed, and annealed at 600°C for 16 hours.

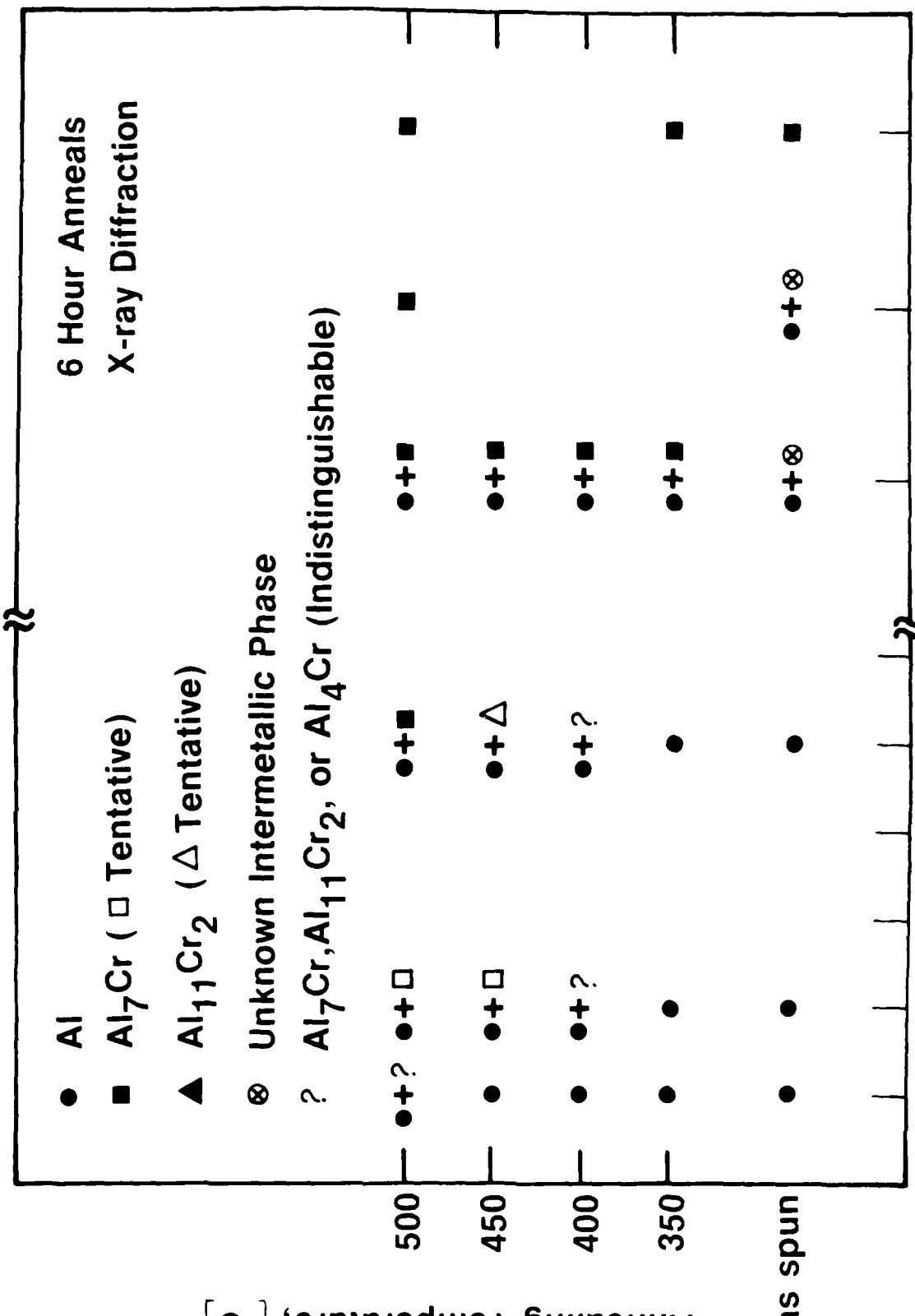

Figure 17. Phases observed by x-ray diffraction in melt-spun and annealed Al-Cr ribbons.

APPENDIX I. LIST OF PUBLICATIONS AND REPORTS

1. D. Shechtman and L. J. Swartzendruber, "Metastable Phases in Rapidly Solidified Aluminum-Rich Aℓ-Fe Alloys," Proceedings of the Materials Research Society, Boston, Ma., USA, November 1982.

2. D. Shechtman, S. D. Ridder and R. Mehrabian, "The Structure of Microparticles made by the MPP Technique, Proceedings of the Third Conference on Rpaid Solidification Processing, National Bureau of Standards, Gaithersburg, Md., USA, December 1982.

3. W. J. Boettinger, R. J. Schaefer, F. Biancaniello and D. Shechtman, "The Effect of Solidification Velocity on the Microstructure of Ag-Cu Alloys," ibid.

4. D. Shechtman, T. Z. Kattamis, F. S. Biancaniello and W. J. Boettinger, "The Microstructure of Rapidly Solidified NiAℓ-Cr Quasibinary Eutectic," ibid.

5. R. J. Schaefer, M. Rosen, J. J. Smith, D. Shechtman and R. Mehrabian, "Nondestructive Characterization of Rapidly Solidified Aℓ-Mn Alloys," ibid.

6. R. J. Schaefer, D. Shechtman and F. S. Biancaniello, "Rapid Solidification Microstructures and Precipitation in Aℓ-Mn Alloys," MRS Meeting, Boston, Ma., November 1983.

7. L. Bendersky and W. J. Boettinger, "Cellular Microstructure in Rapidly Solidified Ag-15 wt% Cu Alloys," Materials Research Society meeting, Boston, Ma., November 1983.

8. D. Shechtman, W. J. Boettinger, T. Z. Kattamis and F. S. Biancaniello, "The Microstructure of Rapidly Solidified NiAℓ-Cr Quasibinary Eutectic," Acta Metall. 32 (1984), 749-756.

9. W. J. Boettinger, D. Shechtman, R. J. Schaefer, and F. S. Biancaniello, "The Effect of Solidification Velocity on the Microstructure of Ag-Cu Alloys," Met. Trans. 15A (1984) 55-66.

10. S. D. Ridder and D. Shechtman, "Microstructure of Supercooled Sub-Micrometer Aluminum-Copper Alloy Powder," ASTM Conference on Rapid Solidification of Aluminum Powders," Philadelphia, Pa., (April 1984).

11. W. J. Boettinger, D. Shechtman, T. Z. Kattamis and R. J. Schaefer, "The Effect of Rapid Solidification Velocity on Microstructure and Phase Stability Extension in NiAℓ-Cr Quasibinary Eutectic," 5th Conference on Rapid Quenching and Solidification of Metals, Sept. 1984, S. Steel and H. Warlimont, eds.

12. D. Shechtman, R. J. Schaefer, and F. S. Biancaniello, "Precipitation in Rapidly Solidified Aℓ-Mn Alloys," accepted for publication in Met. Trans.

13. L. Bendersky, T. Z. Kattamis and F. S. Biancaniello, "An Analytical TEM Study of New Intermetallic Phases in the Co-Sn System," Materials Research Society Meeting, Boston, Ma., November 1984.

14. L. Bendersky, R. J. Schaefer, F. S. Biancaniello and D. Shechtman, "Rapidly Solidified Aℓ-Cr Alloys: Structure and Decomposition Behavior," submitted for publication in Met Trans.

15. L. Bendersky, "Orientation Relationship between Precipitated $A\ell_9(Fe,Ni)_2$ Phase and α-Aluminum," submitted for publciation in Metallurgical Transactions.

16. D. Shechtman and I. Blech, "The Microstructure of Rapidly Solidified $A\ell_6Mn$," submitted for publication in J. of Applied Physics.

17. D. Shechtman, I. Blech, D. Gratias and J. W. Cahn, "A Metallic Phase with Long-Ranged Orientational Order and Broken Translational Symmetry," manuscript in preparation.

REPORTS

1. D. Shechtman and E. Horowitz, "Characterization of Rapidly Solidified Alloys," CMR-RSA-1, November 1981.

2. D. Shechtman and E. Horowitz, "Characterization of Rapidly Solidified Alloys," CMR-DARPA-1, January 1982.

3. D. Shechtman and E. Horowitz, "Characterization of Rapidly Solidified Alloys," CMR-RSA-2, March 1982.

4. D. Shechtman and E. Horowitz, "Characterization of Rapidly Solidified Alloys," CMR-RSA-3, May 1982.

5. D. Shechtman and E. Horowitz, "Characterization of Rapidly Solidified Alloys, CMR-RSA-4, August 1982.

6. D. Shechtman and E. Horowitz, "Characterization of Rapidly Solidified Alloys: Accomplishments, Current Status, and Future Plans," CMR-RSA-5, January 1983.

7. D. Shechtman and E. Horowitz, "Characterization of Rapidly Solidified Alloys," CMR-DARPA-6, February 1983.

8. D. Shechtman and E. Horowitz, "Precipitation in Rapidly Solidified Al-Mn Alloys," CMR-DARPA-7, August 1983.

9. D. Shechtman and E. Horowitz, "Metastable Phases of Rapidly Solidified Al-Rich Al-Fe Alloys," CMR-DARPA-8, January 1984.

10. D. Shechtman and L. Bendersky, "Characterization of Rapidly Solidified Alloys," CMR-DARPA-9, October 1984.